The Dissertation Committee for Shengyuan Zhang
certifies that this is the approved version of the following dissertation:

Effects of Surface Temperature in Gas-Surface Interaction: Quantum-State Resolved Studies of H_2 Scattering from Si(100)

Committee:

Greg O. Sitz, Supervisor

Michael Downer

James L. Erskine

Charles B. Mullins

John W. Keto

Effects of Surface Temperature in Gas-Surface Interaction: Quantum-State Resolved Studies of H_2 Scattering from Si(100)

by

Shengyuan Zhang, B.S.,M.A.

DISSERTATION

Presented to the Faculty of the Graduate School of

The University of Texas at Austin

in Partial Fulfillment

of the Requirements

for the Degree of

DOCTOR OF PHILOSOPHY

THE UNIVERSITY OF TEXAS AT AUSTIN

December 2010

Dedicated to my parents.

Acknowledgments

Foremost, I would like to thank my advisor, Dr. Greg O. Sitz. I would always appreciate his patience for opening the window of surface science to me. His motivation, enthusiasm and knowledge gave me huge support in all the time of my PhD study, research and writing of this dissertation.

Besides my advisor, I would like to thank the rest of my committee: Profs. Michael Downer, James L. Erskine, Charles B. Mullins, John W. Keto, for their time, comments and hard questions.

I want to thank Dr. Leah Shackman and Dr. Jonghyuk Kim for enlightening me a first glance of this research. In addition, I would like thank other students working in the lab over the years. Discussions with them were a great fun during work. They are Rick Hankins, Anne Smith, Robynne Hooper, Elisabeth Siebert, Joel Meyers, Jonathan Ganc, Andrew Hill, Eric Irrgang, Victor Chua, Matthew Wilde. In particular, I enjoyed the working together with long time friend and fellow workmate, Dr. Arban Uka. I would thank the staff in the machine shop, the electronics shop and the cryogenics shop on the third floor for their amazing work and support.

Finally, I would like to thank my wife, who accompanied me through this completion, and my parents, who gave me life and love and carry it through all my life.

Effects of Surface Temperature in Gas-Surface Interaction: Quantum-State Resolved Studies of H_2 Scattering from Si(100)

Publication No. _____

Shengyuan Zhang, Ph.D.
The University of Texas at Austin, 2010

Supervisor: Greg O. Sitz

The scattering of H_2 from Si(100) has been studied using pulsed molecular beam techniques and quantum state-specific detection methods. These studies can be used to test theoretical calculations and give insight into new theories of molecule-surface interactions, a fundamental study in a diverse field of science and technology.

In this work, time-of-flight (TOF) spectra of the elastic scattering of H_2(v=1. J=1) and H_2(v=0, J=1) from clean Si were recorded over a wide range of surface temperatures. Two data processing strategies were developed to extract rich kinematic information from the scattering experiments, e.g., mean translational energy exchange, absolutely survival probability, and angular and speed distribution of the scattered molecules. No such set of quantitative results has been reported before for this system. Compared with close

packed metal surfaces, these scattering experiments from a covalently bonded semiconductor surface showed a completely distinct dynamics, e.g. the finding of energy gain instead of loss from the substrate, much broader angular distribution and some counterintuitive surface temperature effects. From the studies of molecules/surface scattering experiments, the thermal excitation on Si(100) surface which depends on surface temperature can substantially alter the adsorption barrier and its distribution, and therefore changes the kinematics of scattered molecules. As a result, even the most basic understanding of the dynamics has to include phonon excitation and deexcitation of the silicon substrate.

Table of Contents

List of Tables

List of Figures

Chapter 1

Introduction

1.1 Surface Science

Surface Science is the study of physical and chemical phenomena that occur at surfaces. Such phenomena affect virtually all aspects of our daily life. It finds extensive applications in diverse industries, such as the manufacture of fertilizer, fuel cell, automobile exhaust systems and patterning of integrated circuits, in which techniques of catalysis and nanoscience play an important role. Surface science is the foundations of catalysis and nanoscience.

There are many analysis techniques used in the study and analysis of surfaces. These include Auger electron spectroscopy (AES), low-energy electron diffraction (LEED), electron energy loss spectroscopy (EELS), thermal desorption spectroscopy (TDS) and other surface analysis methods. The interfaces are also studied by optical techniques such as second harmonic generation spectroscopy (SHG), Reflection-absorption infrared(IR) and dual polarisation interferometry (DPI). More modern analysis methods include scanning-tunneling microscopy (STM) and all its descendents. All above have their specific applications in different research fields. The molecular beam techniques and optical quantum state-specific method used in our lab are particularly

designed for the study of dynamics of molecule-solid interactions.

1.2 Why H_2-Silicon Scattering?

The semiconductor industry is characterized by rapid development. According to Semiconductor Industry Association (SIA) Industry Fact Sheet(`http://www.sia-online.org/cs/industry_resources/industry_fact_sheet`), in 2005 the semiconductor industry made over 90 million transistors for every man, woman and child on Earth, and by 2010, this number is around 1 billion transistors. The worldwide 2009 sale has grown to $226 Billion. Parallel with the increase in sale, the IC's components have become smaller and smaller. The famous Moore's Law predicts that the number of transistors on a chip doubles every two years.

Because of these facts, the reasons for studying the dynamics of H_2-Silicon interaction are clear. First, silicon is the principal material in semiconductor technology. The hydrogenation of Si is of considerable importance, e.g. for the growth of epitaxial Si layers by chemical vapour deposition from mono- and disilane[21]. Secondly, hydrogen is the simplest molecule allowing for detailed calculations. Furthermore, the (100) and (111) surfaces of Si are well defined and are easy to obtain with high quality. In addition, reaction of H atom on Silicon is straightforward and well understood[2], but for H_2, we don't know much about the nature of the reaction due to its intrinsic complexity. Finally, the interactions of H_2 with various metal surfaces in particular H_2/Cu and H_2/Pd have been intensively studied experimentally [14][50][51][60][61].

Therefore, the H_2/Si experiment can be considered an extension of these previous studies.

Just like in high energy physics/particle physics, the collision or the scattering experiment in surface science is the single most powerful tool for investigating the structure and interaction of our research objects. In this type of experiment, one fires a stream of "bullets", such as H_2 in our case, at a target object, such as Si, Cu, Pd etc, and by observing the change of quantum state, energy and distribution of angular and velocity of the bullets", one can gain information of the target object and its interaction with the bullets. This kind of information gives theorists direct test of their theory calculations and can inspire new assumptions or approximations.

The foregoing can be considered as motivation to study the scattering experiment of H_2 on Si. From now on, we will concentrate on H_2 and Silicon. In the next section reconstruction of Si(100) surface will be introduced.

1.3 Reconstruction of Clean Si(100) surface

Silicon is the second most abundant element in the earth[1]. Silicon occurs mostly in the form of compounds. It very rarely occurs as pure free element in nature. For technological reasons, high quality single crystal silicon has been massively produced.

[1]The eighth most abundant element in the universe as we know so far. The chemical composition of earth is quite different from that of the universe

A single crystal silicon, like other group IV insulators and semiconductors including diamond and germanium, forms as the face-centered diamond cubic crystal structure with a lattice constant, 5.430710 Å [39] shown in Fig. 1.1. The covalent bonds are 2.35 Å long and each has a bond strength of 2.34 eV [57]. Select low index planes are shown in Fig. 1.2.

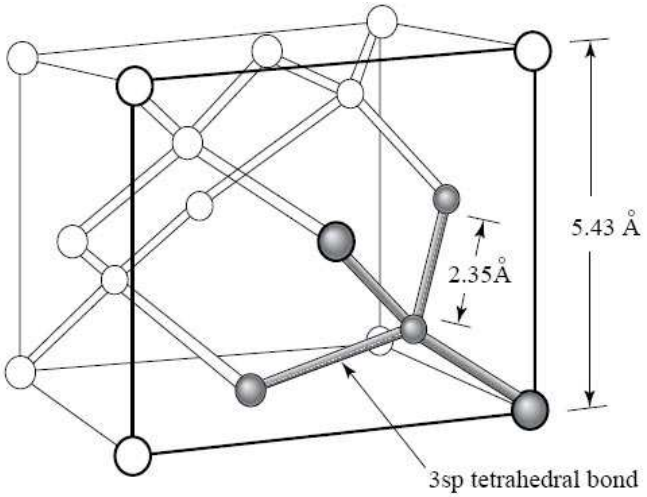

Figure 1.1: Unit cell of the diamond cubic structure showing the lattice constant, 5.43 Å, bond length, 2.35 Å and locations of Si-Si bonds.

In most cases the surface atoms have a different structure than that of the bulk. When a surface is introduced by terminating the crystal along a given plane, the atoms at the surface or near the surface plane can't keep their original equilibrium positions since they no longer experience inter-atomic forces from one direction. To lower the surface energy, the atoms near the surface assume positions with different spacing and/or symmetry from the bulk atoms, creating a different surface structure. This phenomenon is normally

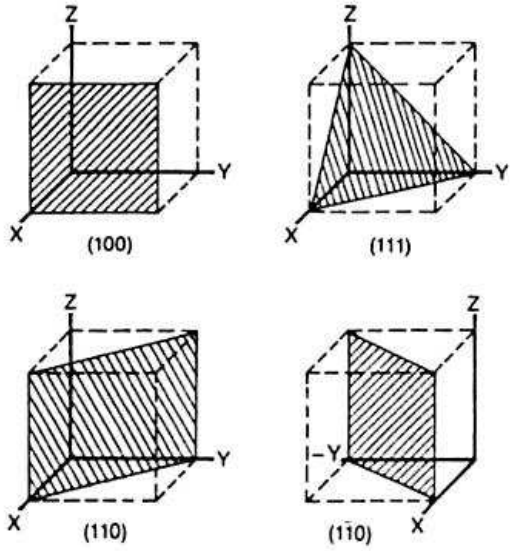

Figure 1.2: Examples of low-index planes.

categorized as a reconstruction or a relaxation. [2]

The commonly accepted model for the reconstructed Si(100) surface is the dimer model. It was first proposed by Schlier and Farnsworth after they observed a (2x1) LEED pattern instead of (1x1) one [48], the result of a square unit cell which the Si(100) planes have. Compare the difference between ideal and reconstructed Si(100) surfaces in Fig. 1.3 [17].

This symmetric model was modified by Levine [32] and later by Chadi [9], who proposed that the dimer should be asymmetric or buckled. A buckled

[2]There is some difference in concept between relaxation and reconstruction. Relaxation is a small and subtle rearrangement of the surface layers without change in the periodicity parallel to the surface or to the symmetry of the surface. It is common on metal surface. In contrast, the reconstruction of surfaces involve larger, yet still atomic scale, displacements of the surface atoms. It is more prevalent on semiconductor surfaces. [37]

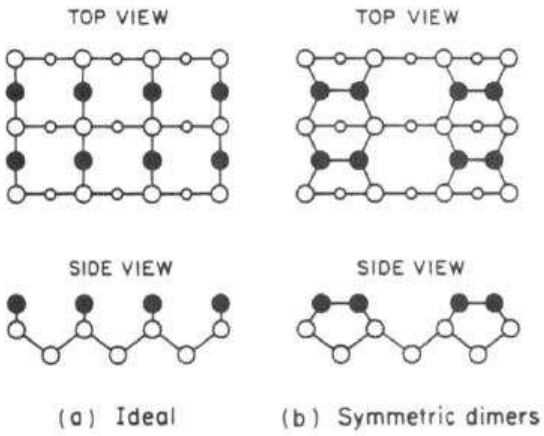

Figure 1.3: Top and side views of ideal and reconstructed Si(100) surfaces [17].

dimer can be achieved by pushing one end of the dimer down and lifting the other end up. Many experiments [22] [29] and theoretical calculations [38] [27]have been devoted to answering one question: is the dimer a symmetric or buckled one? Most of them point toward buckled dimer.

This is not the end of the story. Depending on the relative ordering of the buckled dimer, different configurations are obtained as shown in Fig. 1.4[58]. In Fig. 1.4a the (2x1) structure corresponds to symmetric dimers. Figure 1.4b shows the buckled dimers in the same direction. However, theory calculations state that adjacent dimers in a row are expected to buckle in opposite directions to further relax the surface lattice strain; two different orderings of these buckled rows are possible. In Fig. 1.4c a local p(2x2) is obtained if the neighboring rows are in the same direction, while in Fig. 1.4d a local c(4x2) is obtained if the neighboring rows are in opposite directions.

In the previous calculations, the c(4x2) buckled dimers has a lower surface energy in an amount of 0.140 eV/dimer compared with the symmetric (2x1) dimers [38] [27] and the total energy difference between c(4x2) and p(2x2) is 1.2 meV/dimer [20].

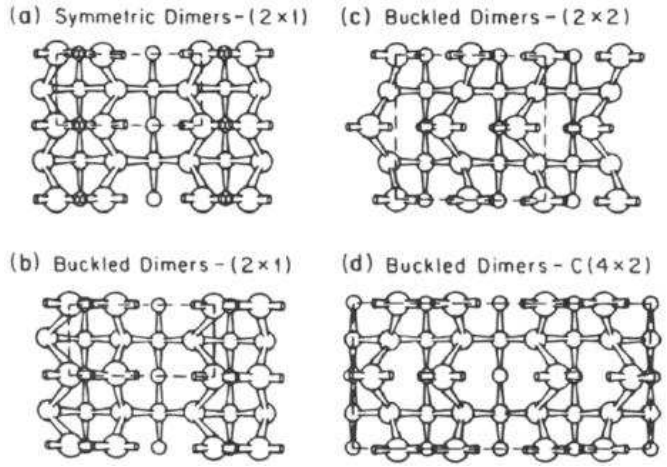

Figure 1.4: Schematic Diagrams for the possible configurations of surface dimers on the reconstructed Si(100) surface. [17]

From these experimental and theoretical studies, it was widely accepted in 1990sthat the buckled dimers construct a c(4x2) structure as the ground state. [3] The most stable structure of clean Si(100) between 80 K and 140 K is confirmed to be the c(4x2) configuration by scanning tunneling microscopy (STM) studies. There is still some controversy for observations below 80 K. C(4x2), p(2x2) even symmetric dimer p(2x1) structure had been observed

[3]To describe surface structure in terms of Wood's notion, "p" in p(2x2) means "primitive",which is often omitted; "c" in c(4x2) means "centred".

[26][40][46]. Final agreement has not been reached yet but that topic is out of our concerns. Several low-energy electron diffraction (LEED) measurements [28] confirmed a reversible second-order phase transition between the disordered p(2x1) and ordered c(4x2) phases that occurs around 200 K. The p(2x1) phase observed by STM at room temperature was attributed to the quick flip-flop motion of the buckled dimers [20] [41].

A typical STM image of Si(100) surface is shown on Fig. 1.5. "Nothing is perfect." The Si(100) surface is not perfectly flat. The dimer rows on consecutive terraces separated by single-layer height steps are perpendicular to each other. The Si(100) sample we studied is not one domain but two. We will discuss this later.

1.4 Small sticking coefficients–experimental approach

The H_2/Si adsorption experiment was first conducted by Law at the Bell laboratories almost 50 years ago[30]. His data shown in Fig. 1.6 showed that the sticking coefficient of H_2 on Si is extremely small, say, below 10^{-9} under common experimental condition.[4] The results has been confirmed by more modern TPD studies by Liehr and co-workers for the Si(100) surface[33]. For a very long time until 1990s, the sticking coefficient of H_2 on Si under common experimental condition was considered to be "immeasurably" small.

[4]The higher sticking coefficient, up to 10^{-6}, in Law's data may be due to the initial adsorption on steps or defect sites which is saturated after a coverage of 2% is reached. Further adsorption after that is below 10^{-9}.

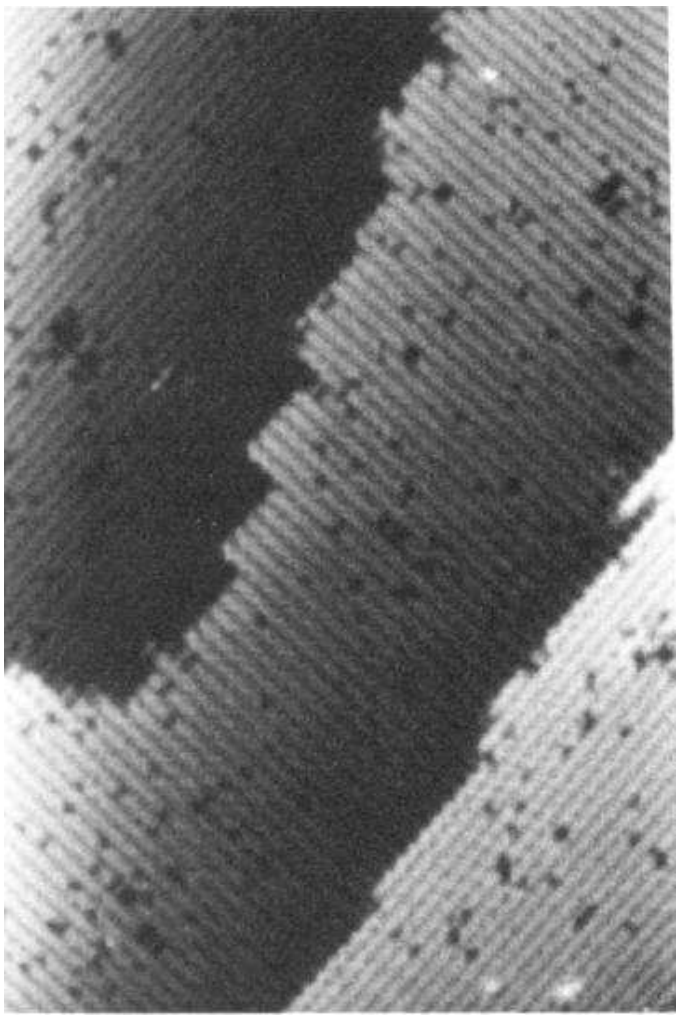

Figure 1.5: STM image of single-layer stepped Si(100) surface. The dimer rows in two domains are perpendicular to each other [56].

5

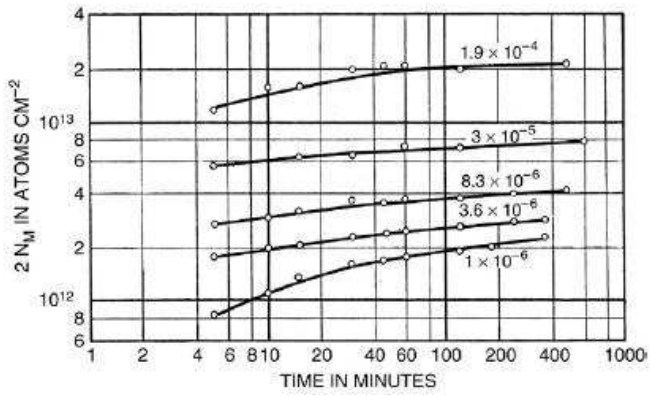

Figure 1.6: Adsorption of H_2 on the surface of single-crystal Si filaments as function of time at varying pressure (in torr) after Law [30]. Given that a monolayer of adsorbate has 0.678×10^{15} molecules/cm^2 on Si surface, the increase by 10^{12} atoms/cm^2 observed between 100 and 500 min for a pressure of 3×10^{-5} Torr, which is equal to 7.2×10^5 Langmuir, and corresponds to sticking coefficient of 10^{-9}.

Law's work turned out to be the most sensitive and accurate investigation of the sticking coefficient of H_2/Si for quite some time until the use of optical second harmonic generation (SHG). This new experimental approach was demonstrated by Downer and coworker [19] by monitoring the hydrogen coverage during silane adsorption and hydrogen desorption during epitaxial growth on Si(100) and by Bratu and Höfer [3] by monitoring the H_2 and D_2 adsorption on Si (100). As a purely optical, but nevertheless surface sensitive technique, it allows one to monitor adsorbate coverage in real time. An ar-

[5]One Langmuir (symbol:L), which is equal to an exposure of pressure 1×10^{-6} Torr during 1 s corresponds to a gas flux of $1.62 \times 10^{15} H_2$ molecules/s/cm^2.

rhenius plot of the initial sticking coefficients for dissociative adsorption of H_2 and D_2 on Si(100)(2x1) surfaces is shown in Fig. 1.7 for data from Bratu and Höfer [3]. Fitting to an exponential temperature dependence gives a result of $E_{\text{ads}} = 0.75 \pm 0.1$ eV for H_2 adsorption on Si(100)(2x1).

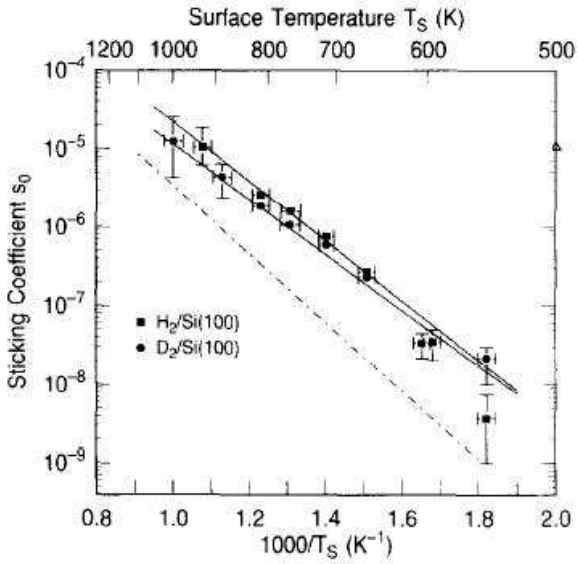

Figure 1.7: Arrhenius plot of the initial sticking coefficients for dissociative adsorption of H_2 and D_2 on Si(100)(2x1) surfaces[3]. The full symbols indicate the values derived for H_2 and D_2 on Si(100)(2x1). The solid lines are the result of a fit to an exponential temperature dependence, $s_0 = A\exp(-E_{\text{ads}}/kT_s,)$ with$A = 1 \times 10^{-1\pm0.5}(4 \times 10^{-2\pm o.5})$ and $E_{\text{ads}} = 0.75 \pm 0.1(0.70 \pm 0.1)eV$ for H_2 (and D_2), respectively.

Although molecular hydrogen does not readily dissociate on Si surfaces, the reaction is energetically favorable, since the dissociation energy of H_2 is considerably smaller than the Si-H bond energy. A schematic diagram that illustrates the energetic situation in adsorption and desorption is shown in

Fig. 1.8 and the relevant energies for Si(001)(2x1) are collected in Table 1.1 [12]. If we consider Fig. 1.8 to be the reaction path through a multidimensional potential energy surface (PES), then the activation energy or the dissociation barrier from E_{ads} is consistent with the experimental result of the small sticking coefficient: For $E_{\mathrm{ads}} = 0.6$ eV, the Boltzmann-factor $\exp(-E_{\mathrm{ads}}/k_B T)$ is equal to approximately 10^{-10} at room temperature, i.e. only a fraction of $10^{-10)}$ of the thermally distributed H_2 has enough kinetic energy to overcome the barrier and stick on the surface. This number will be further reduced due to molecules hitting the surface with wrong/non-ideal impact parameters.

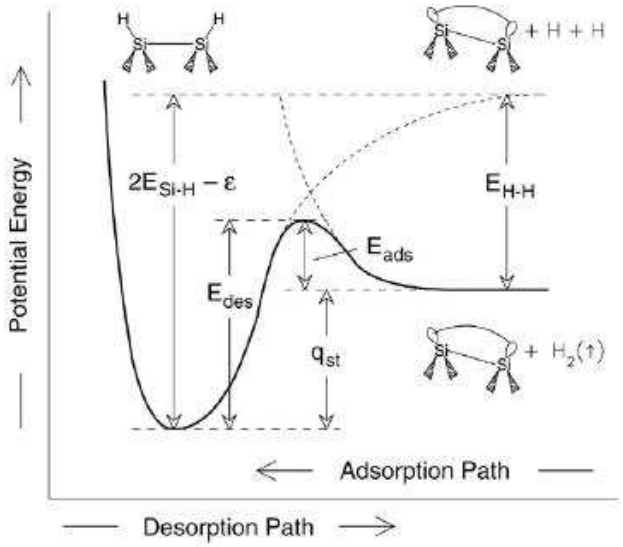

Figure 1.8: Schematic 1-dimensional energy diagram for recombinative desorption and dissociative adsorption of H_2/Si(001) [12].

One goal of our experiments is to study the scattering of state prepared H_2 from Si as a function of surface temperature. In principle we could perform

Table 1.1: Experimental values of the H_2 dissociation energy $E_{\text{H-H}}$, the activation energy for recombinative desorption E_{des} and the chemisorption energy q_{st} for hydrogen on Si(100)(2x1). The Si-H bond energies $E_{\text{Si-H}}$ and the adsorption barrier E_{ads} are given in terms of differences between these values: $E_{\text{Si-H}} = 1/2(q_{st} + E_{H-H}), E_{\text{ads}} = E_{\text{des}} - q_{st}$.

	Si(100)(2x1)	reference
$E_{\text{H-H}}$(eV)	4.478	[52]
E_{des}(eV)	2.48 ± 0.1	[18]
q_{st}(eV)	1.9 ± 0.3	[44]
$E_{\text{Si-H}}$(eV)	3.2	
E_{ads}(eV)	0.6	

scattering measurements and look for loss of reflected intensity that resulted from adsorption even at temperatures well above the desorption temperature.

1.5 Effects of Surface Temperature–Theory

The one-dimensional potential energy curves, such as the one shown in Fig. 1.8, that go back to the fundamental work of Lennard-Jones [31], can prove to be of great value in discussion and highlight the problem but have severe limitations and must be used for illustrative purposes only. They do not lend themselves to generalization when more than one coordinate is necessary to specify a configuration. Since the potential does not include other important degrees of freedom, like the H-H distance that changes during dissociation or the orientation of molecule and its impact parameter on the surface, it cannot account for most of the interesting dynamical effects. For example, when we use this simple picture of H_2 interaction with Si surfaces described by

Fig. 1.8 to understand the results of the reverse reaction, dissociative adsorption, performed by Kolasinski and coworkers in 1994, it just simply fails[25]. When molecules desorbs across a large adsorption barrier their kinetic energy is expected to be the order this barrier height. This is what occurs for H_2/Cu. But for Si there was essentially no heating at all. This surprising result was called the "barrier puzzle" and simulated most of the work on Si/H during the next two decades. [6]

Molecule-surface reactions are complex many-body problems involving many electrons and nuclei. In general, theoretical approaches to these kinds of problems involve two steps. First, we need to know how to describe the interaction potential between the molecule and the surface atoms, in other words, we have to solve the electronic structure problem. This is not trivial. Remember that when we switch our problem from the Schrödinger equation of hydrogen atom to that of H_2 molecule how difficult the problem has become. It can only be resolved numerically by means of the iterative self-consistent field method(SCF) or Hartree-Fock method. This involves many approximations. The Born-Oppenheimer approximation is usually applied first. After the electronic structure problem is solved, the PES is given by the ground-state energies for the molecule-surface system for all possible atomic configurations. Second we must solve the molecular dynamics using quantum mechanics, classical or semi-classical depending on the system we are studying. Which de-

[6]"barrier puzzle" is understood when an appropriate distribution $E_{\mathrm{ads}}(E_0, W)$ is considered, E_0, the mean barrier height, and W, the distribution width arising, e.g. from molecules incident at different lattice impact parameters and with different orientations.

scription is suitable for our problem is essentially a question of the magnitudes of de Broglie wavelength and energy transfer. For H_2, the de Broglie wavelengths at room temperature is a few Angstrom which is comparable to the Si lattice constant. Apparently the Si/H system should be considered quantum mechanically for complete understanding. When more degrees of freedom are involved, the problem can be scarily difficult and quantum methods sometimes becomes intractable. In this case classical or semi-classical methods have to be introduced and the results have to carefully examined.

Above is a general description of this problem's theoretical approach. As far as H_2/Si is concerned, theoretical methods including quantum chemical configurational interaction (CI) calculations on clusters, density functional theoretical techniques (DFT) on clusters and slabs, and Quantum Monte Carlo (QMC) calculations for the potential energy surfaces (PES) and quantum mechanical as well as classical reaction dynamics calculations on such PES have recently unraveled a rather complex reaction scenario.

In the case of H_2 adsorption on metal surfaces, Cu or Pd etc., the substrate was typically considered to be static, at least in a first approximation. This is not appropriate in the case of Si/H_2. The rearrangement of substrate Si atoms has to be taken into account. For some experimental parameters, the reaction dynamics is even dominated by the substrate degrees of freedom as we can see from the experimental result in Fig. 1.7. This conclusion is consistent with Brenig and Hilf's 7-D calculated result shown in Fig. 1.9.

The dynamics of adsorption/desorption reactions can be described quite

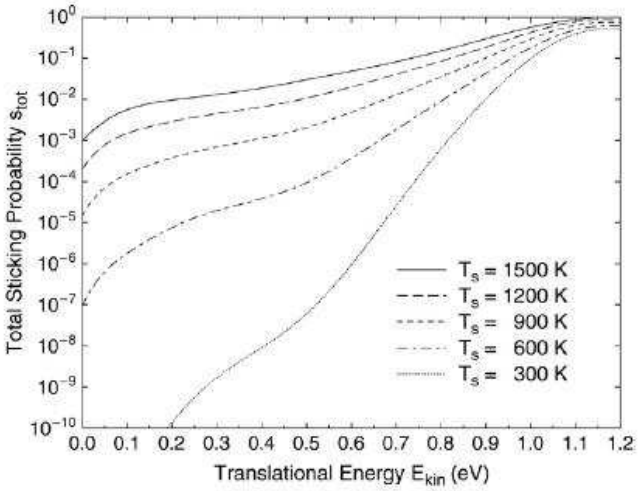

Figure 1.9: Sticking coefficient for the adsorption of molecular hydrogen on silicon as function of kinetic energy for various surface temperatures as predicted by the model of Brenig et al.[6]

well in terms of a 7-D Hamiltonian including one surface phonon mode in addition to the 6-D molecular Hamiltonian.[6]. In Brenig's 7-D model, the one surface degree of freedom is not defined specifically. Even the six degrees of freedom of H_2 are based on the abstract reaction coordinates. For this reason, the details of the reaction mechanism leading to the observed strong increase of sticking coefficients with temperature are not known. The geometry and motion of Si surface atoms change with surface temperature. That results in the change of adsorption barrier, its distribution and thus the change of the kinematics of scattered molecules. The goal of the present work is to study experimentally the effects of surface temperature in H_2/Si(100) interaction to uncover new behaviors and inspire new theories.

Chapter 2

Experiment Set-Up

In this chapter the general experimental set-up used in all the scattering experiments will be discussed along with details relevant to the Si/H_2 experiment particularly the Si surface's treatment and tests to guarantee a clean, well-ordered surface.

2.1 Overview

This whole apparatus has been built up over the past two decades. Several upgrades were added/replaced in this apparatus during my work in the lab, such as the new main chamber lid whose rotation is now easily controlled by a computer, and a high-duty turbo pump, which replaced the old liquid Nitrogen trapped diffusion pump.

A schematic diagram of the experimental apparatus is shown in Fig. 2.1. The apparatus consists of three differentially pumped chambers, source chamber, main chamber and buffer chamber in between. A supersonic H_2 beam exits a pulsed nozzle, operating at 10 Hz, in the source chamber. After the beam passes through the skimmer, the "narrowed" beam comes into the buffer chamber. In the buffer chamber, the beam is chopped by a high-speed ro-

tating disk, which has narrow slits to allow the beam to pass through. Only a small part can escape the chopper and enter the main chamber through a specially shaped aperture. Finally, the well-defined pulse reaches the single crystal target and scatters off the target surface. This single crystal is held on a manipulator, which is attached to the lid on top of the main chamber. The lid is placed on two differentially pumped seals and a bearing so it can be rotated to any position which is manipulated by a high-duty step motor and controlled by a labview program. The target can then been easily and accurately rotated into position for ion sputtering, low energy electron diffraction (LEED), [1] or scattering experiments.

2.2 Pumping and probing of H_2

All experiments described in this work were performed with a fraction of the incident H_2 molecules pumped from (v=0,j=1) to the (v=1,j=1) state. The technique used for this molecules quantum state preparation is called "Raman State Preparation Technique" and the laser beam is called the pump beam, which intersects the molecular beam before the probe laser. The pump beam is produced by passing the 532 nm light from the second harmonic of a pulsed Nd:YAG laser into a "Raman cell" filled with H_2 at a pressure of 65 psi. Part of the light undergoes Raman scattering from the H_2 molecules. The Raman-Shifted light along with the residual fundamental light together

[1] This assembling is also used for auger electron spectroscopy(AES) and electron energy loss spectroscopy.

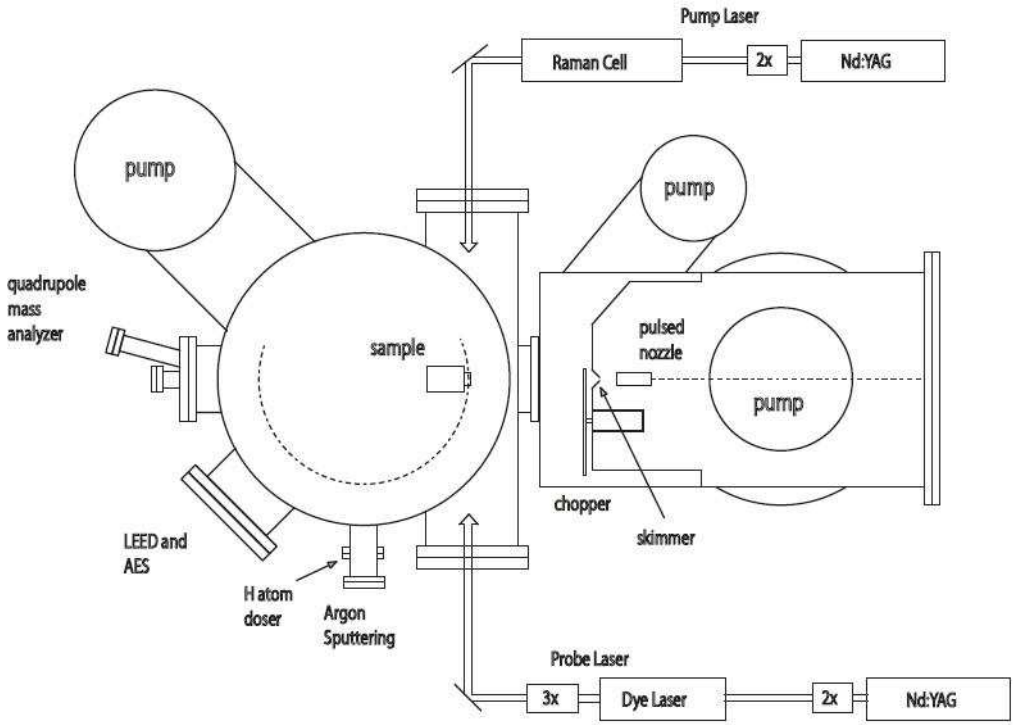

Figure 2.1: Schematic diagram of the experiment set-up, top view.

form the pump beam which is directed over to the main chamber. The pump beam is focused on the molecular beam of H_2 to excite the molecules into the first vibrational state, (v=0)→(v=1) through the stimulated Raman scattering. Since the energy difference between the vibrational ground state (v=0) and the vibrationally excited state (v=1) is around 0.5 eV, the H_2 population of vibrational excited state (v=1) at room temperature is almost zero. The pumping process can transfer part of the ground state molecules into the excited state ones. The percentage of transformation strongly depends on the pump laser intensity. Watts [59] measured the population of the (v=1,j=1) state as well as the removed population from the (v=0,j=1) state which is shown in Fig. 2.2[2]. The Raman state preparation technique was used to study state transition of the excited state molecules which interact with surface in most previous students' work. In my work, the main advantage is that it supplies a far better time and space resolution to allow the studies the molecules' angular and velocity distribution since the time scale of this pumped pulse is much shorter than that of the thermal molecular beam, 0.054 μs compared to 7.3 μs. More details will be discussed in Appendix A.

To detect the incident and scattered molecules, a second laser beam called the "probe" beam is used. The probe beam is produced by Nd:YAG laser, dye Laser and two optical crystals, KDP and BBO. First The dye laser

[2]The most populated state of H_2 at room temperature is (v=0,j=1). Selection rules allow only $\Delta J = 0, \pm 2$ with linearly polarized incoming laser the Q branch is stronger than S branch. Therefore, the Stimulated Raman Scattering (SRS) enhances mostly the transition between (v=0,j=1) →(v=1,j=1) states[4].

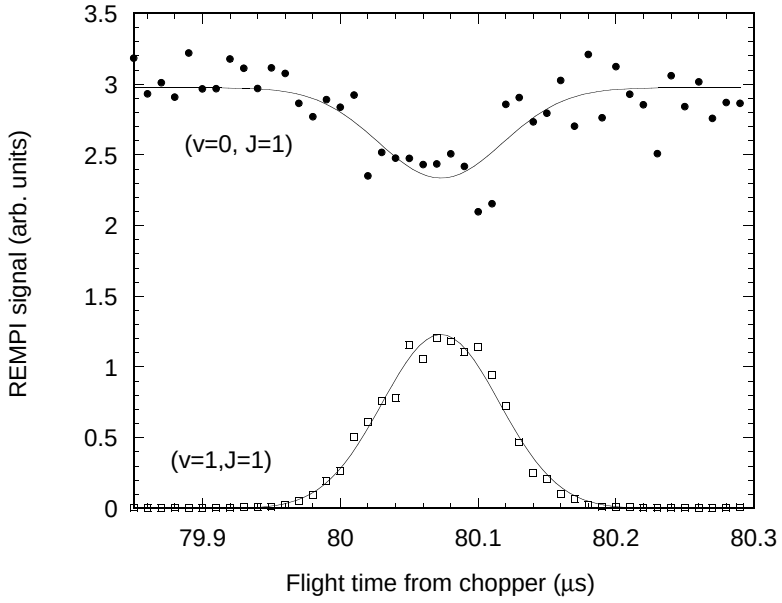

Figure 2.2: Comparison of the changes of populations in two state,(v=0,j=1) and (v=1,j=1) as a result of the Raman pumping process. Original data from [59]

is pumped by the frequency doubled Nd:YAG laser. The dye laser light is frequency tunable. The dye laser light is then frequency doubled, using a potassium dihydrogen phosphate (KDP) crystal. The frequency doubled light is mixed with the fundamental light, using a beta-barium borate (BBO) crystal, to produce the third harmonic of the dye laser light. Finally, the ultra-violet light is focused into the molecular beam. Using the tunable ultra-violet light we can state-selectively ionize the H_2 molecules using 2+1 resonance-enhanced multiphoton ionization (REMPI). The molecules are resonantly excited from the original electronic state, in our case, the (v=1,j=1), to the E,F excited electronic state by two ultra-violet photons, using $E,F^1\Sigma_g^+ \longleftarrow X^1\Sigma_u^+$. A third photon ionizes the molecules which are already in this excited electronic state , as shown in Fig. 2.3[34].

These ions are collected by a channel electron multiplier array (CEMA) plate by applying appropriate steering high voltages. This small current is amplified, integrated and acquired by computer. This way we count the number of ions.

In the scattering experiment, the pump laser works like a "marker" which put marks on the molecules we want to study. The probe laser works like a "detector" which observes the "marked" molecules only. This is the case as least for Si/H_2 due to two reasons: a, the most populated state of H_2 is (v=0, j=1) and very rare H_2(v=1,j=1) exist; b, once molecules are pumped to excited state (v=1, j=1), almost all molecules are scattered back without

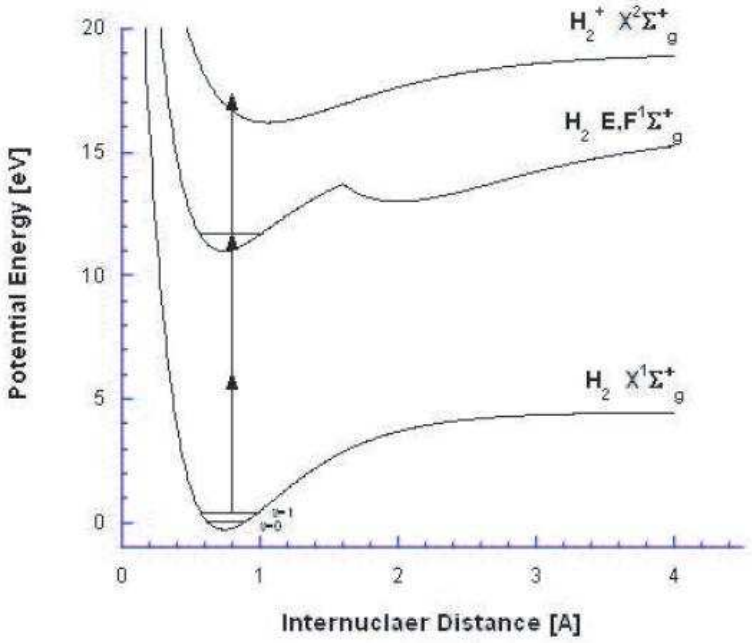

Figure 2.3: 2+1 REMPI. Two photons excite the state selectively to E,F$^1\Sigma_g^+$ state through a virtual state, then a third photon ionizes the excited hydrogen molecule.

state change[3]. Both the pulsed pump laser and probe laser have a pulse length of $\approx 10ns$ which allow enough time and space resolution for our purpose. Figure 2.4 gives a close-up view around where the molecular beam interacts with the surface. In this experiment, two focused lasers are placed 0.25-1.25 mm before the surface. When we study the scattering of H_2 molecules in (v=1,j=1)state, we place the probe laser between the pump laser and Si; by contrast, we place the probe laser before the pump laser and the surface when molecules in (v=0,j=1) are studies.

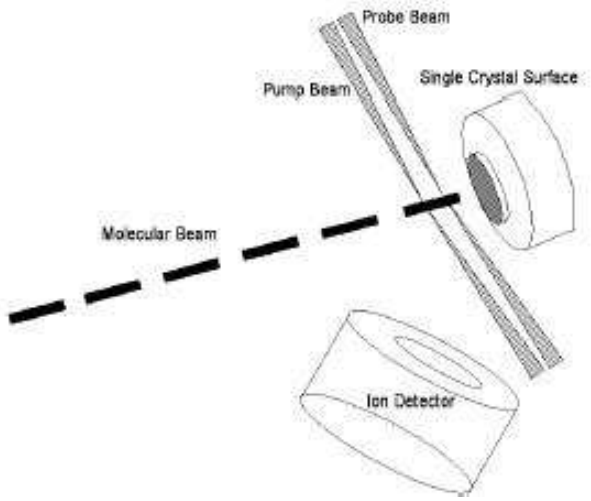

Figure 2.4: close-up view around where the molecular beam interacts with the surface. Sample, probe laser, pump laser, molecular beam and CEMA are present.

The timing in this experiment is crucial. A schematic diagram is shown

[3]From Chapter 4, the survival probability is close to 1.

in Fig. 2.5. Everything starts from a reference timing signal trigged by an LED-phototransistor on the chopper when one of four slits (two narrow and two broad) passes it. This signal is sent to the nozzle, the gated signal-integration circuit board, pump laser and probe laser after a series of appropriate delay operations. Among them one sophisticated digital delay generator is used for both Nd:YAG lasers' Q-switch, so timing accuracy is guaranteed to an accuracy of 1 ns. For other parts analog delay generators are used, which suffice for the timing requirement.

2.3 Measurements

The sample is heated from the rear by electron bombardment emitted from a 2% thoriated tungsten filament and is cooled conductively by liquid nitrogen. In the experiment, the temperature ranges from 100K to 900K, even to 1300K when heating to clean the Si sample. Thermal expansion is unavoidable and unpredictable for such change of temperature since the expansion comes from not only the sample itself but also the sample holder and even the connection between sample holder and the lid of the main chamber. We can't wait for the whole assembly to reach a thermal equilibrium as the sample surface will be contaminated by residual molecules in the main chamber. As a result the sample's position can change in the order of a few μm during an experiment, and that can cause a huge error in data analysis if carelessly treated. Different strategies are used to study the scattering properties of two different quantum state molecules. After these careful operations, the error

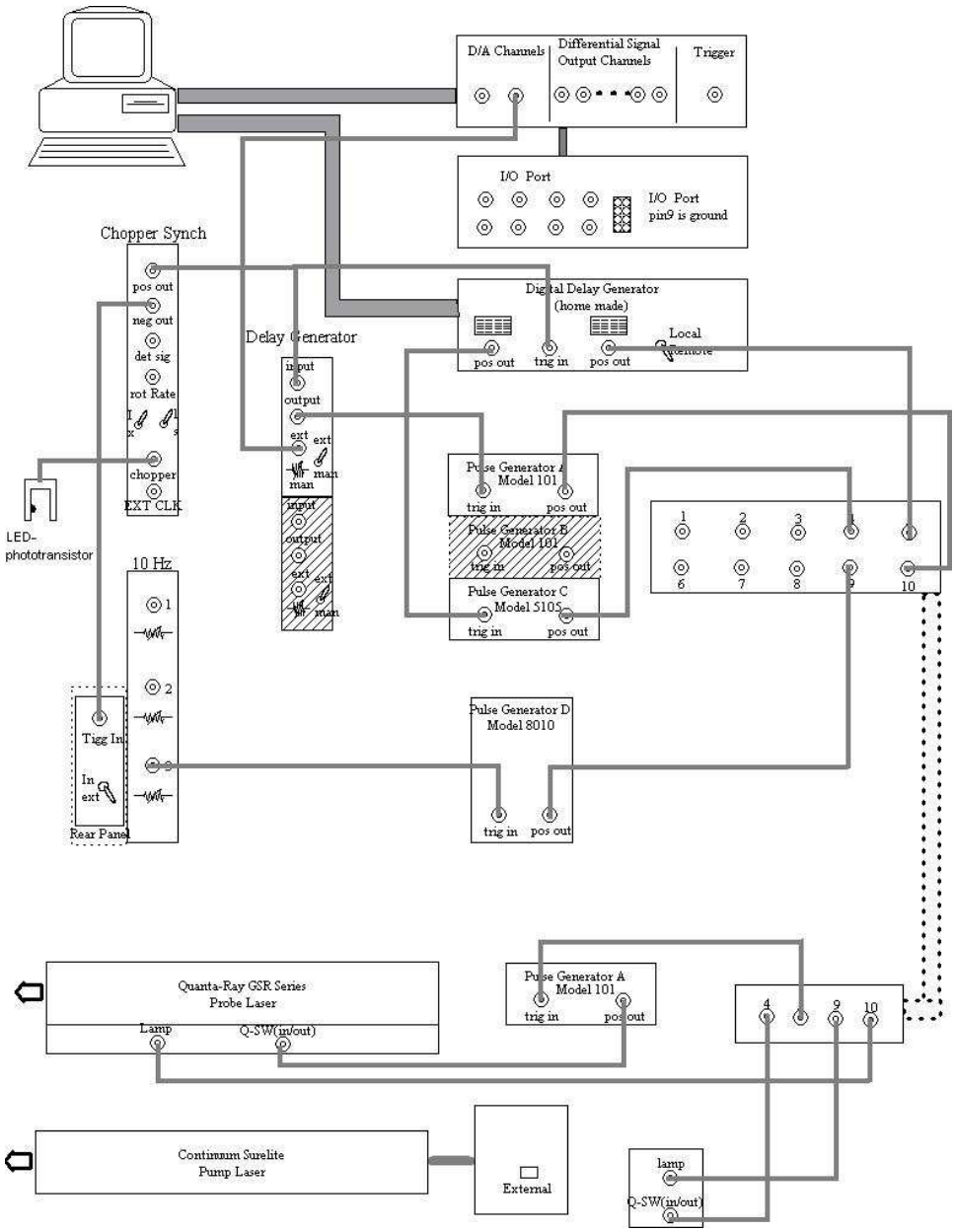

Figure 2.5: Schematic diagram of timing control.

caused by thermal expansion can be reduced to obtain reasonable results. In previous studies of Metal/Molecule scattering experiments, this may not be a big concern, since the temperature range is not that much. For Si/H_2, we need to treat them cautiously.

Basically only one type of measurement is made in both experiments: a time of flight(TOF) measurement. In this measurement, the firing time of the probe laser is scanned in a step of 10 ns while the firing time of pump laser is fixed. The ion signal is measured for each delay time.

2.3.1 Scattering of H_2(v=1, j=1) from Si

When scattering of H_2(v=1,j=1) is studied, the probe laser is placed between pump laser and sample surface as shown in Fig. 2.6b. For one TOF scan both the incident and scattered signals are measured simultaneously. A series of TOF measurements are obtained by changing the probe laser position horizontally or vertically relative to the direction of the molecular beam. The information on the molecules' velocity and quantum state survival probability is obtained. More details are presented in chapter 4.

2.3.2 Scattering of H_2(v=0, j=1) from Si

For this study the probe laser is placed before pump laser and sample surface. The pump laser is 0.033 inch close to sample surface and probe is 0.006 - 0.008 inch away from probe laser as shown in Fig. 2.6a. So the signal we observed reflects the changes of H_2 in (v=0,j=1) after scattering from

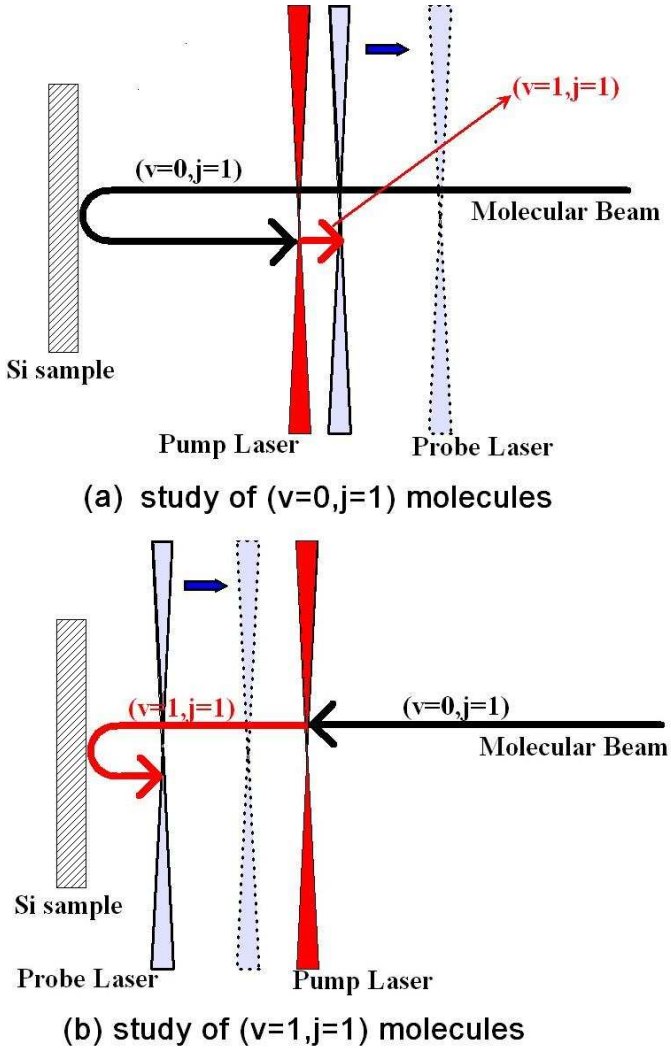

Figure 2.6: Schematic diagram of the positions of pump laser (red) and probe laser (black) in two different experiments. The molecular beam in black line represents molecules in (v=0,j=1) state; in contrast, the molecular beam in red line represents molecules in (v=1,j=1) state after pumped by pump laser. (a) shows the scattering of (v=0,j=1) molecules (b) shows the scattering of (v=1,j=1) molecules.

the Si surface. One advantage of this setup in this measurement is that the thermal expansion isn't an issue any more. Once the two positions of the pump laser and probe laser are fixed, small position shift of the Si sample due to thermal nonequilibrium won't cause significant change of signal given other conditions are unchanged. This is always true if the sample's size is large enough [4] when it is compared with the distance between the surface and probe laser. Time-of-flight spectra are recorded and these data are fit to a simulation model whose parameters describe the velocity and angular distribution of the scattered molecules. This will be discussed in detail in chapter 5. For this simulation model some parameters must be extracted from the incident beam in advance. When the incident beam is studied, the probe laser is placed between pump laser and sample surface, the same setup as we do for studies of scattering of H_2(v=1,j=1), that is introduced above.

[4]The Si sample's size is 0.45 *times*0.45 inch.

Chapter 3

Pre-Experimental Studies

In the molecule surface scattering experiment ultra high vacuum is required to maintain a contamination-free environment for the duration of the experiment. Studies of the main chamber residual gas become necessary. As far as Si is concerned, several questions have to be answered beforehand, such as "what is the main contamination?", "How to clean the Si surface?", "How to determine the cleanliness and surface order of Si?". All questions above will be answered in this chapter.

3.1 Main chamber residual gas analysis

Total pressure in the main chamber is 2×10^{-9} Torr measured by a ion gauge. To further reduce the total pressure a liquid nitrogen trap cylinder and a titanium sublimation pump (TSP)[1] are available. The total pressure can be reduced to 4×10^{-10} Torr. A comparison of the mass spectrum with/without the liquid nitrogen trap is shown in Fig. 3.1, that shows the partial pressure of water drops 85%. The residual gases in the scattering chamber (main chamber)

[1]We will see the liquid nitrogen trap efficiently pumps down water. The TSP is not used in our experiment.

are monitored by a quadrupole mass spectrometer (QMS). The main residual gases are hydrogen (m/e=2), water (m/e=18), carbon monoxide and nitrogen (m/e=28), and carbon dioxide (m/e=44). A $H_2(m/z = 2)$ signal around 600 ^oC‘ is found in a series of TPD experiments even if no dosing of H atom is done. When the liquid nitrogen trap is applied, this signal is compressed significantly, as shown in Fig. 3.2. In addition, when the silicon sample is removed from the main chamber, this signal is gone, which proves that the signal is coming from the silicon surface. Since molecular hydrogen has a very small reactivity on Si under common experimental environment, the residual gas, H_2O, is the sole source. This is consistent with Schmeisser and Flores's studies and experimental results of H_2O on silicon that indicates at room temperature the sticking coefficient of H_2O on Si(100) is high (near unity) and constant up to saturation[43][63]. The decomposition product H_2 was observed also in their TPD experiments. The H_2 desorption temperature they observed is around 800K which is the same as that of H_2 desorption from hydrogen covered Si surfaces. The same TPD experimental results are shown in Fig. 3.2, that suggests that H_2 desorption occurs from Si sites.

The liquid nitrogen trap is necessary for this experiment. The partial pressure of water based on our calculations is around 1×10^{-10} Torr after the Liquid nitrogen trap is applied, that allows enough time to complete a series of scattering measurements before a significant amount of H_2O is accumulated on the surface. During experiments the Si surface was cleaned approximately every hour. The procedure and measurements for Si sample is introduced next

section.

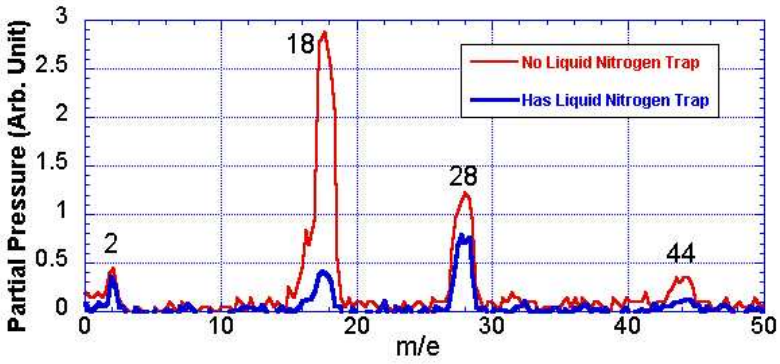

Figure 3.1: A comparison of the mass spectrum in the main chamber with/without the liquid nitrogen trap. Spectra show that the partial pressure of Water (m/e=18) downs 85%.

3.2 Si surface preparation and characterization

The sample surface used is a 0.45×0.45 inch single crystal Si(100)(p-type, Boron doped, $10 - 20\Omega \cdot$ cm, thickness:525 ± 25 μm)[2]. The surface is heated by electron bombardment from a 2% thoriated tungsten filament located behind the sample and attached on a sample holder made from molybdenum. Some updates of the temperature control feed-back circuit designed by Michael Gostein were made to supply up to 150 mA emission current to heat the sample up to 1300 K. The thermocouple is very easily shorted at

[2]Doping concentration for this sample is 1^{15} cm^{-3}. Compared with silicon's atomic density of 5×10^{22} atoms per cm^3, this still gives a purity greater than 99.99999%.

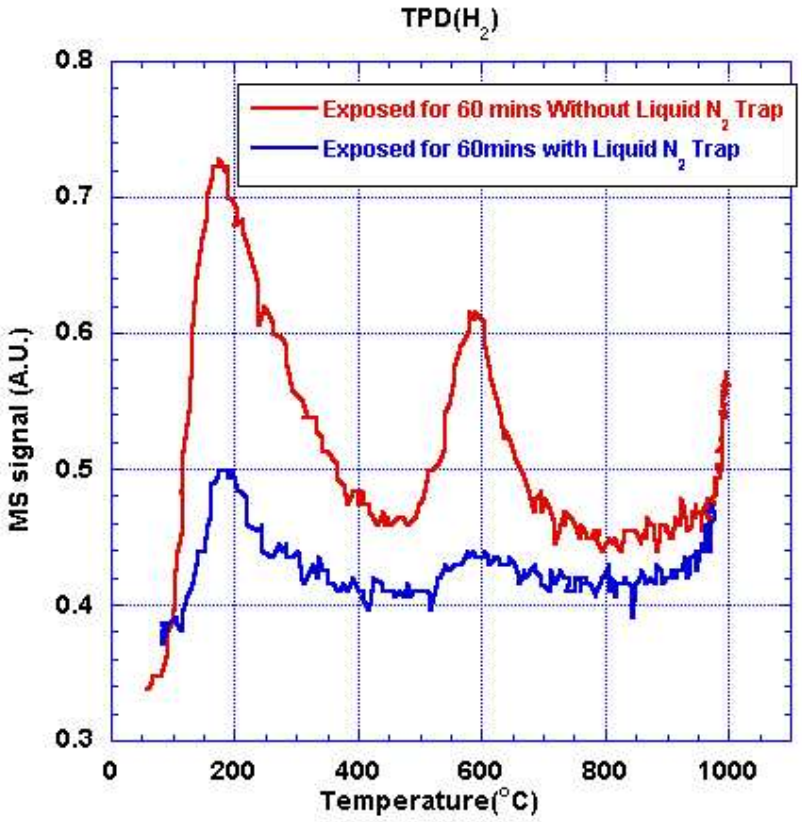

Figure 3.2: A $H_2(m/z = 2)$ signal around 600 ^{o}C is found in TPD experiment even no dosing of H atom. When the liquid nitrogen trap is applied, the signal is compressed significantly.

such a high temperature. A new type thermocouple with special sheath material other than stainless steel replaced the old ones after several failure. The sample is cooled by conductance by a cryostat using liquid nitrogen.

A very shallow layer (approximately 1 nm or 10 Å) of so-called native oxide is formed on the surface when silicon is exposed to air. This "thick" oxide must be removed before conducting the experiment. In addition, due to the existence of the residual gases of H_2O and O_2, the Si surface has to be cleaned every one hour[3]. The procedure is simple[12][42]. Heating up to 1300 K can remove the surface oxide completely. An Auger Spectrum and TPD experiments proved the procedure's efficiency. The following paragraph is a quote from Chung's book, "Practical guide to surface science and spectroscopy":[11]

> A SiO_2 layer is formed on top of pure silicon. The Auger peak of silicon is at 91eV. After oxidation, it is shifted to 78 eV. Therefore, pure and oxidized silicon are easily distinguishable. When the surface is oxidized, the silicon 91 eV peak intensity decreases because of attenuation by the silicon dioxide layer. After a layer of SiO_2 is formed, the 91 eV Auger peak drops to 15% of its clean surface value.

The Auger electron spectrum we measured is shown in Fig. 3.3 is consistent with above statement. Figure 3.4 shows the corresponding heating strategy. In

[3]Other residual gases, like H_2,CO,CO_2 and N_2, don't have too much effects on the experiment. Traditional clean routine, like Ar Sputtering applied on metal surface for removing carbon, is not used for Si surface.

Fig. 3.3 two different Si surfaces, a clean surface and a oxidized surface, have very different Auger electron spectra(AES). The change of AES was clearly observed and began when Si sample was heated above 820 ^{o}C. The Si 91 eV signal became stronger and stronger while more and more SiO_2 was removed until a clean Si surface without any impurity was exposed. The strong clean Si surface signal can last for several hours without noticeable change of the AES signal. But a silicon oxide layer can build up to the same level in several days. To be safe, the surface was cleaned every one hour during the scattering experiments.

The orientation of the single crystal Si was checked using low energy electron diffraction (LEED) as shown in Fig. 3.5. The LEED pattern shows that the reconstruction, which has a 2×1 periodicity exists which are oriented along different crystallographic axes. Keep in mind that the sample used in the experiment has two coexistent "domains". This pattern can last for a few days after a complete cleaning process. There is no LEED pattern with the existence of a disordered silicon oxide layer.

3.3 Hydrogen-Terminated Si Surface

Each Silicon atom on the reconstructed Si(100) surface has one dangling bond. When Si-Si bonds which create the dimer, are broken, each silicon has two dangling bonds. So Sakurai and Hagstrum in 1976 proposed two different hydrogen terminations[47]: the monohydride phase where the dimers are preserved, i.e. the (2x1) reconstruction is preserved, and the one dangling

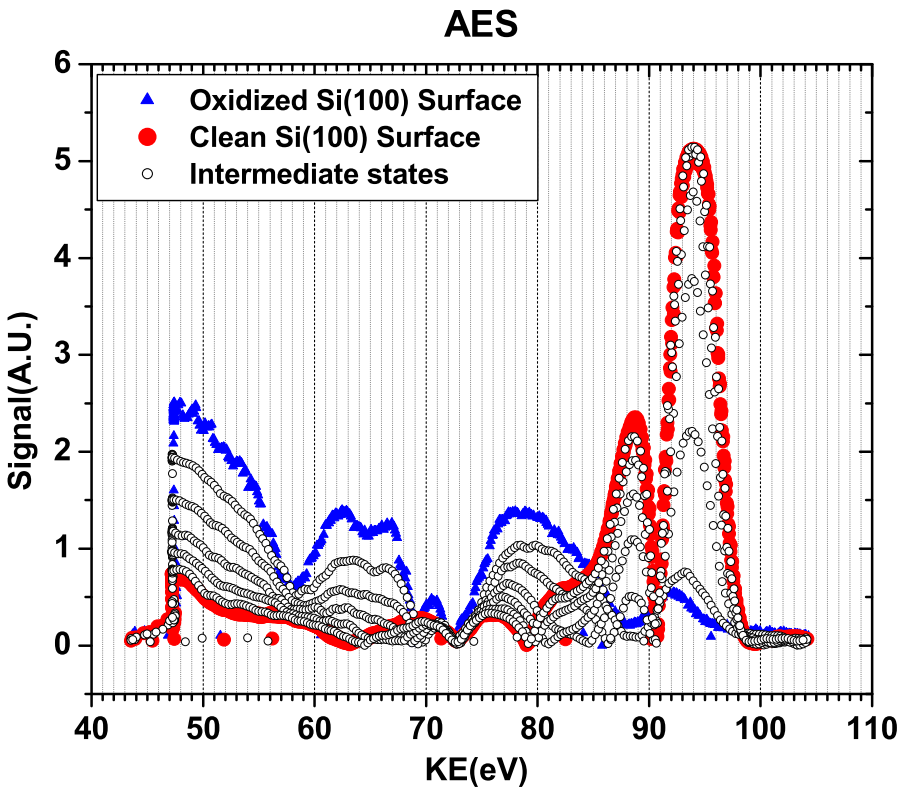

Figure 3.3: Auger electron spectrum changes dramatically when the oxidized Si surface is converted into a clean Si surface. The data with blue solid triangles show the AES of Si sample with a oxidized surface (blue sold triangle), with a clean surface(red solid circle) and the transition state between two different surfaces(blank circle) is shown.

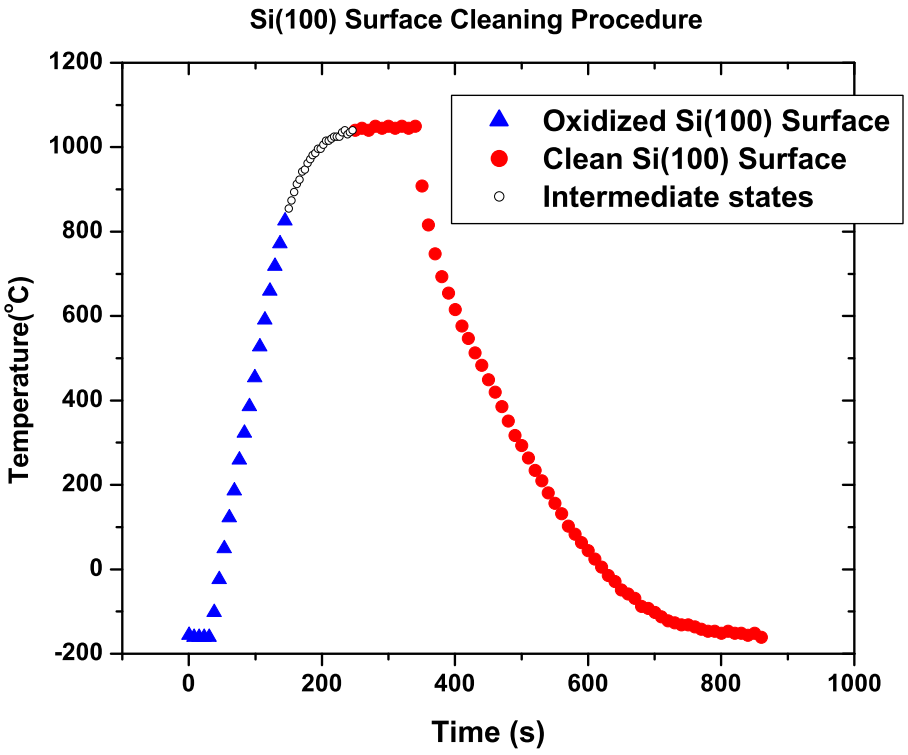

Figure 3.4: The heating up and cooling down schedule used in both TPD experiment and cleaning process. The data (solid circles, red solid triangle, blank circle) correspond to different surface states respectively as shown in Fig. 3.3.

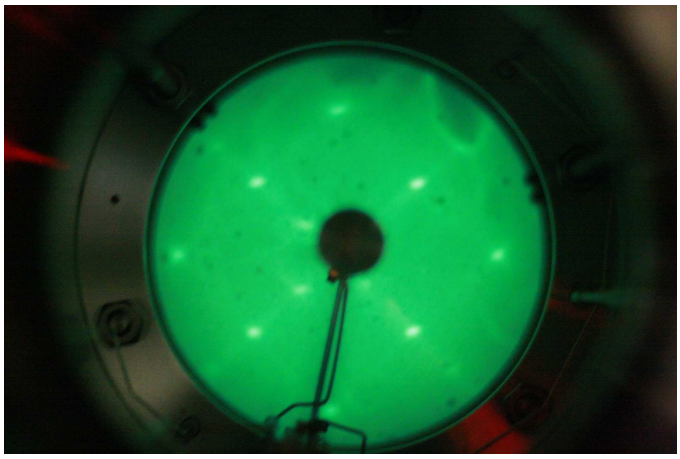

Figure 3.5: LEED pattern of the Si surface. The pattern shows that the surface reconstruction has a 2x1 periodicity and sample used in our experiment has two coexistent "domains".

bonds on each silicon atom are capped by one hydrogen (Fig. 3.6a) and the dihydride phase where the dimer bonds are broken and the two dangling bonds on each silicon atom are capped with two hydrogen atoms(Fig. 3.6b), leading to (1x1) structure. Another intermediate structure was reported by Chabal and Raghavachari in 1985: the (3x 1) structure[8]. Cheng and Yates in 1991 used their results of TPD (shown in Fig. 3.7) and LEED's studies of H-induced surface structure on Si(100) to question the (1x1) structure[10]. Their work shows that while the (3x1) phase consists of mainly monohydride and dihydride structure, the (1x1) phase is in fact composed of a mixture of monohydride, dihydride, and trihydride surface species. This is contrary to the (1x1) model shown in Fig. 3.6b which has a uniform dihydride overlayer. The trihydride surface species lead to the release of $\beta_3 - H_2$ during thermal desorption, which

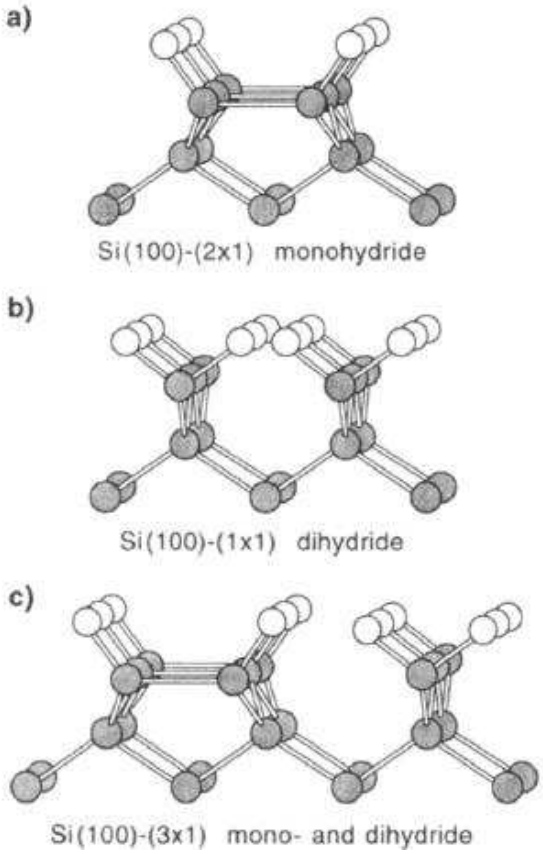

Figure 3.6: Hydrogen-terminated Si(100) surfaces: (a)monohydride, (2x1) structure; (b) dihydride, (1x1) structure;(c) (3x1) structure.[58]

happens around 200K.

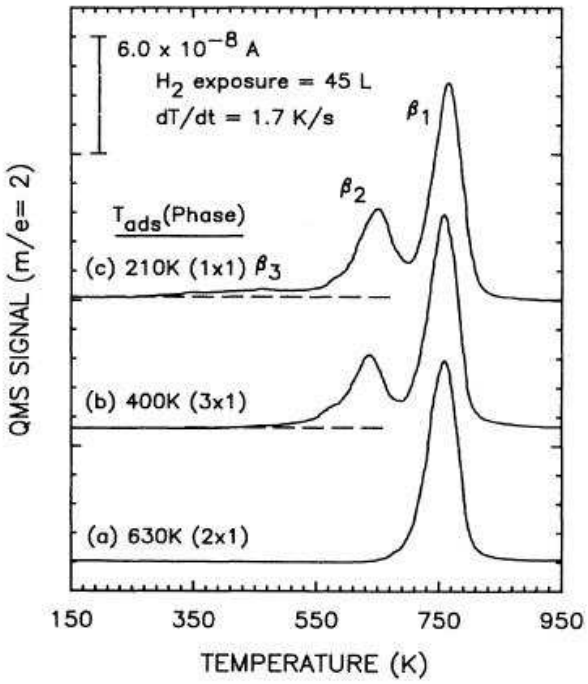

Figure 3.7: TPD spectra of H_2 desorption obtained from H-saturated Si(100) at different adsorption temperatures:(a)630 K,(b)400 K,(c)210 K. TPD spectra were taken with a heating rate of 1.7 K/s after the crystal was cooled down to 130 K.[10]

The methods of preparing hydrogenated silicon surface haven't changed much since the pioneering work of Boland in the early 1990s. A tungsten plate at a temperature above 2500 K (2.6 V input in our set-up)is used to thermally dissociate molecular hydrogen into atomic hydrogen. Atomic hydrogen has high reactivity with the Si surface which creates a hydrogenated silicon surface. To prepare different structured hydrogenated silicon surfaces is like cooking.

Different recipes make different flavored dishes. The adjustable parameters in our case are the temperature of the tungsten filament, hydrogen pressure, duration, and most importantly, surface temperature. The sample temperature was chosen following Cheng's work[10]. Our TPD result is shown in Fig. 3.8. It is consistent with the results in the literature. In the (3x1) structure two peaks around 625 ^{o}C and 425 ^{o}C correspond to the desorption of β_1 H_2 and β_2 H_2. In the (2x1) structure only one peak around 625 ^{o}C shows the desorption of β_1 H_2. Hydrogen atoms can't accumulate on the surface at temperature higher than 550 ^{o}C. A trick when terminating the hydrogenation that was suggested by Mayne and Dujardin [35] was followed. The critical moment occurs when terminating the hydrogenation, in particular, for Si(100)(2x1) surface, First we have to stop heating the sample, second stop the hot filament and finally shut off the hydrogen to the chamber. If all three were stopped at the same time, half the hydrogen adsorbed on the surface would be thermally desorbed since the silicon surface was at 270 ^{o}C. On the other hand, don't wait longer than 30s to turn off the hot filament after beginning cooling the sample, otherwise, the (3x1) reconstruction forms in significant quantity since this is stable at a lower temperature (which is seen when adsorption at 127 ^{o}C) rather than the (2x1) surface as desired.

The H_2 partial pressure during dosing is kept at 10^{-8} Torr. We change the dosing duration to control the exposure. A series of TPD experiments were done with different exposure. The results are shown in Fig. 3.9. The dosing of hydrogen atom is more efficient than suggested by calculation of the

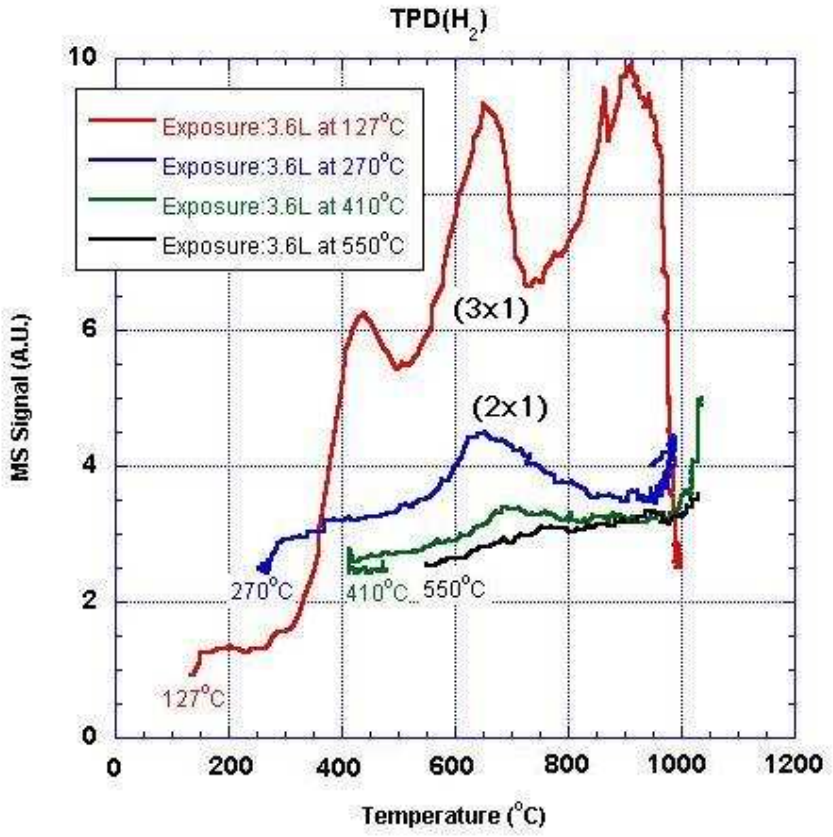

Figure 3.8: TPD spectra of H_2 obtained from H-saturated Si(100) at different adsorption temperatures:(a)127 ^{o}C,(b)270 ^{o}C,(c)410 ^{o}C,(d)555 ^{o}C. TPD spectra were taken with a heating rate of 10K/s after 3.6 Langmuir exposure.

exposure, the product of H_2 partial pressure and time. The reason is that we have no way to estimate the flux of hydrogen atoms dissociated by the hot tungsten plate. The mass spectrometer/ion gauge reads only the "averaged" pressure. The hydrogen atom flux towards the sample is much higher than that around the mass spectrometer/ion gauge. Since the signals don't change so much especially for the β_1 signal. We are expecting a saturation of hydrogen even after 0.66 Langmuir exposures.

Preparing of hydrogenated silicon surface and the following TPD experiments have two purposes:

1. We checked the recipes from other groups' studies of preparing the different hydrogenated Si(100) surfaces, such as (3x1) structure phase and (2x1) structure phase etc., which may be used for further studies of scattering of H_2 on hydrogenated silicon surface.

2. By comparing our TPD experiments results with others' published results, in addition to the results of AES and LEED, our results' consistency assured us that the experimental conditions were satisfied for Si/H_2 studies.

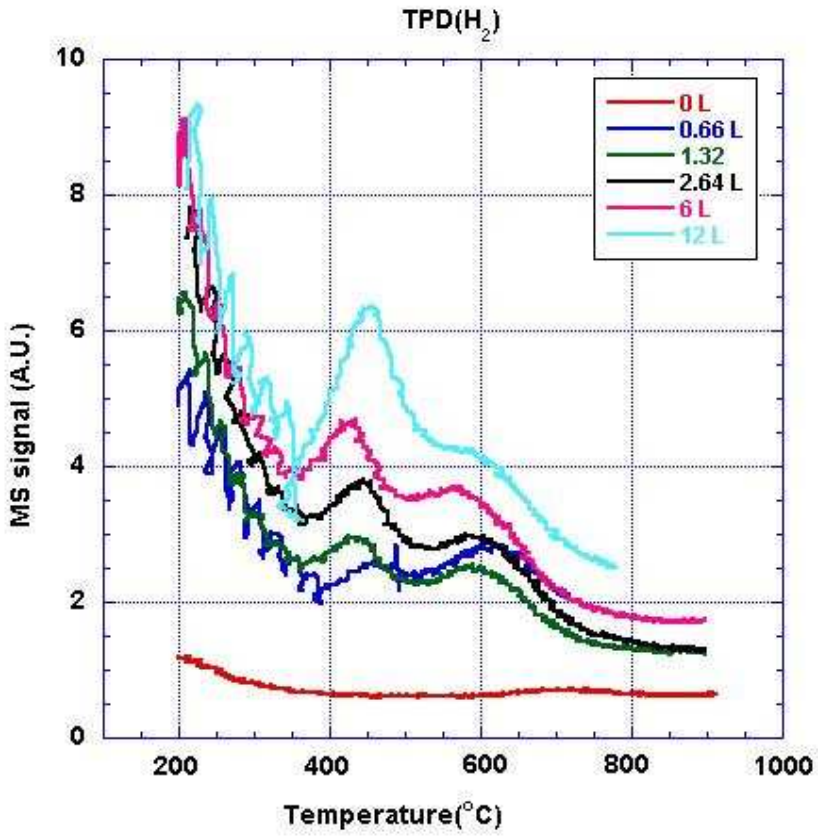

Figure 3.9: TPD spectra of H_2 vs exposure. TPD spectra were taken with a heating rate of 10 K/s after the crystal was cooled down to -165 ^{o}C.

Chapter 4

Elastic Scattering of H_2(v=1, j=1) from Si

We will discuss the experimental results carried out on the H_2/Si(100) system in this chapter for H_2(v=1,j=1)- the vibrational exited state and next chapter for H_2(v=0,j=1) ground state. It has been pointed out that the dissociative adsorption of molecular hydrogen on silicon is a highly activated chemical reaction. The adsorption energy, $E_{\rm ads}$, equals 0.6 eV. Under our experimental condition the reaction possibility is extremely low mainly due to the low incident translational energy, 0.074 ± 0.003 eV and low surface temperature. This condition is illustrated in Fig. 4.1a[24]. Our experimental results find that the survival probability of H_2(v=1,j=1) upon scattering from Si(100) is close to 1 at both low and high temperature. We focus our work on the translational energy exchange, angular and velocity distributions, and survival probability for H_2 in these two quantum states upon scattering from clean Si(100) surface[1].

[1]In molecules/surface dynamics terminology, the scattering can be either elastic (the internal quantum states of the molecules are not changed) or inelastic (the internal quantum states of the molecules are changed). This is a little different from the definition used in classical mechanics.

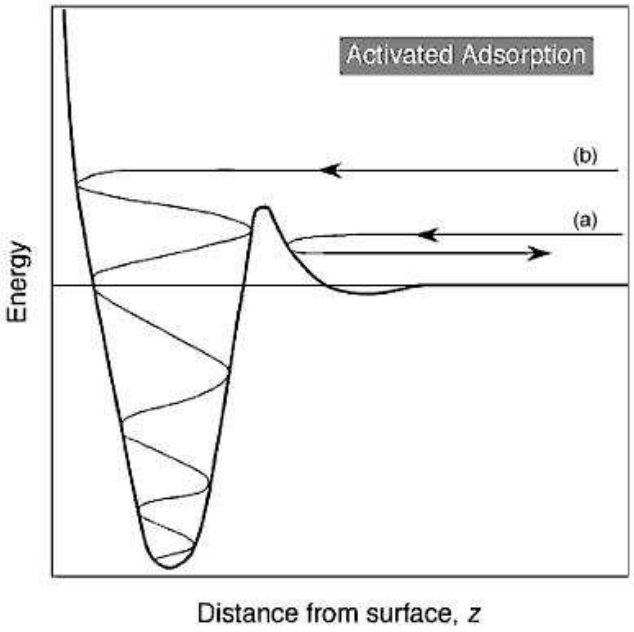

Figure 4.1: Lennard-Jones diagram. A barrier separating the chemisorption well from the gas phase distinguishes activated adsorption. The energy of two hypothetical trajectories are shown in the diagram. (a)low (our case) and (b) high kinetic energy. Classically, only high energy trajectories can overcome the adsorption barrier[24].

4.1 Translational Energy Change

4.1.1 Measurements and Data Processes

The mean translational energy of the incident and scattered H_2(v=1, j=1) molecules can be determined, for each surface temperature, from a series of TOF measurements by changing the probe laser position along the molecular beam axis (see Fig. 2.6). Sample experimental data are shown in Fig. 4.2. Each TOF is for a different probe position and these scans have been offset vertically for clarity. A 3-D visualization and a contour map of these data are shown in Figures 4.3 and 4.4. The big peak at early time in each scan is from the incident molecules and the smaller peak at later time is from the scattered molecules. Due to the narrow velocity distribution and collimation for the incident molecules, the incident curves of all scans are almost identical except for a shift along time and have a Gaussian-like shape, while for the scattered molecules, the signal goes down as the distance between the probe laser and sample increases and has a characteristic asymmetric shape.

The incident beam TOF spectra are fitted to a Gaussian Profile while the scattered beam TOF spectra are fitted to a model as shown in Fig. 4.5. This is the first step of the data processing to convert the density-weighted TOF spectra to flux-weighted one as explained in Appendix B. Experimental data are well reproduced as a smoothed function of time and peak times for the incident/scattered molecules are obtained from the fitting results. In Fig. 4.5, the broad velocity and angular distributions are responsible for the asymmetric shape of the scattered beam profile in the TOF measurement, which has a long

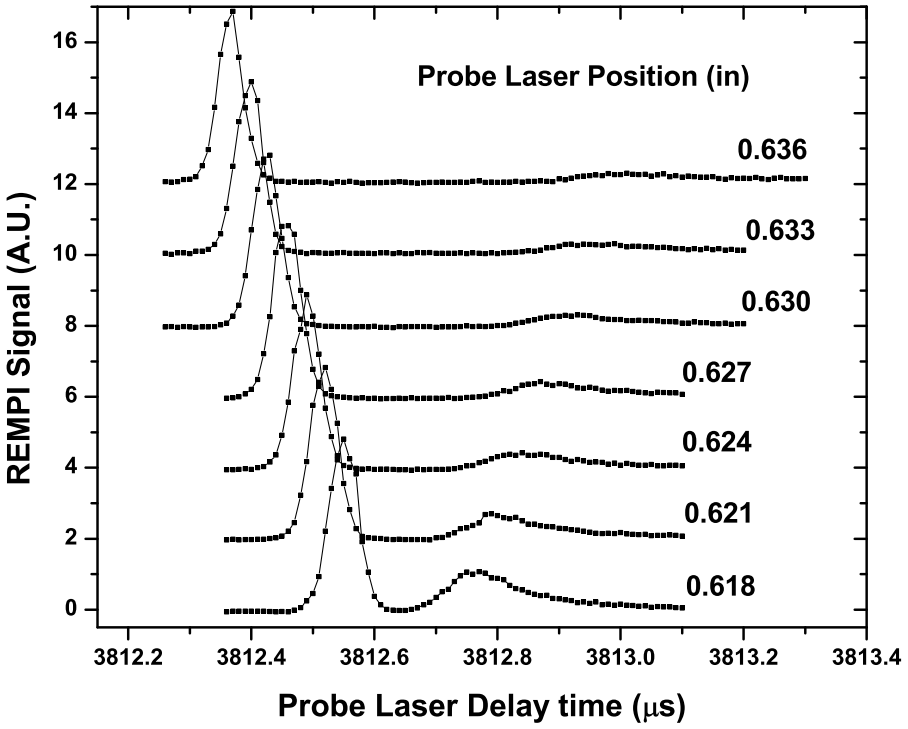

Figure 4.2: A series of TOF measurements of pumped H_2(v=1,j=1) elastic scattering from clean Si(100)(2x1) surface in different probe positions.

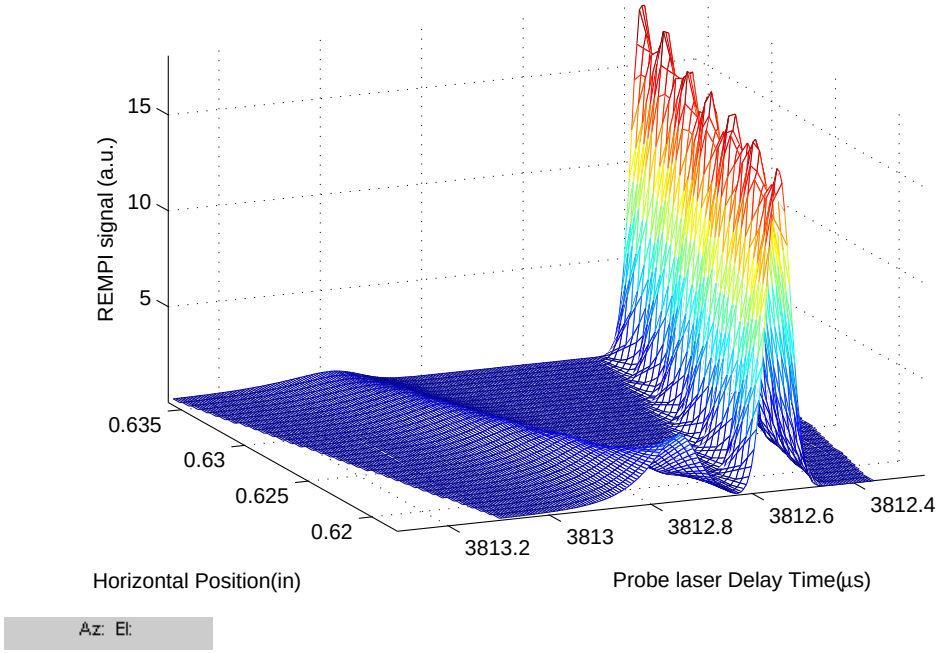

Figure 4.3: 3D visualization of the data shown as in Fig. 4.5.

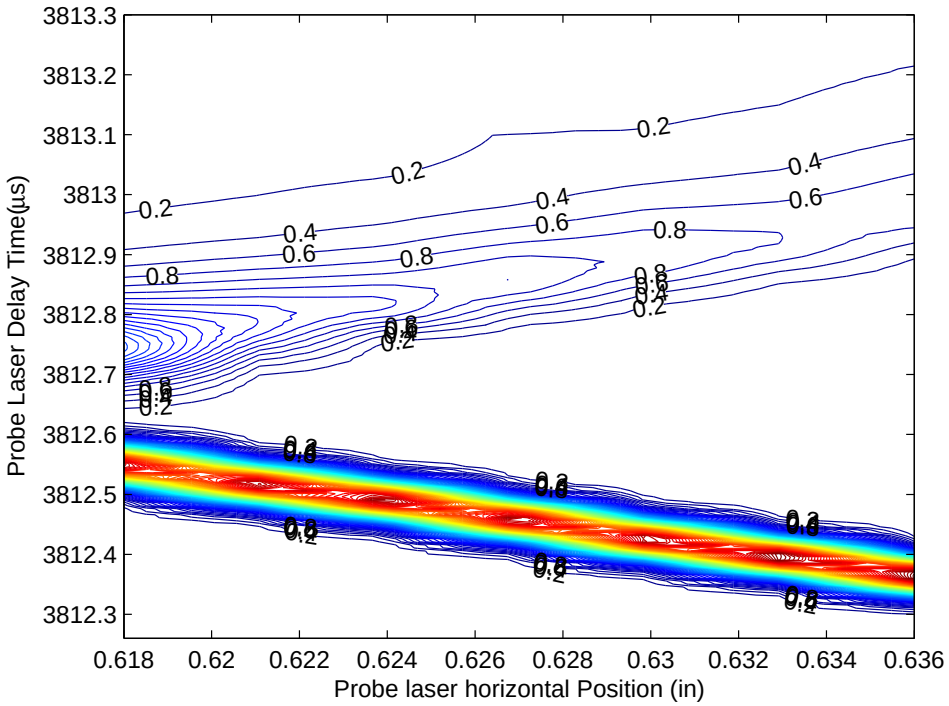

Figure 4.4: The contour map for the data shown as in Fig. 4.6.

tail. Molecules with lower velocities or scattered at larger angles are detected later by the probe laser after scattering back from the sample surface than those with higher velocity and normal scattering, and that gives rise to the asymmetric scattered peak shape.

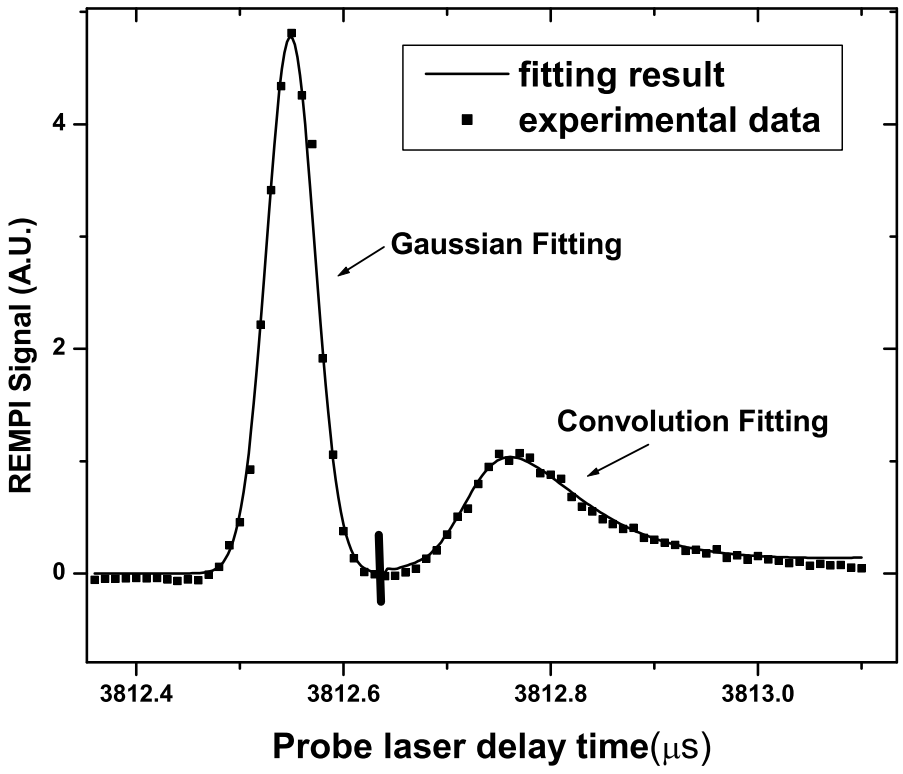

Figure 4.5: The incident beam are fits to a Gaussian Profile while the scattered beam are fits to a model which is explained in Appendix B.

The inverse slopes of the linear fittings of the peak times versus probe position give the incident/scattered mean translational energy. The intersec-

tion of incident and scattered lines gives the surface position along the probe laser translational stage and the peak arrival time of the impinging molecules on the surface. One sample of such measurements are shown in Fig. 4.6.

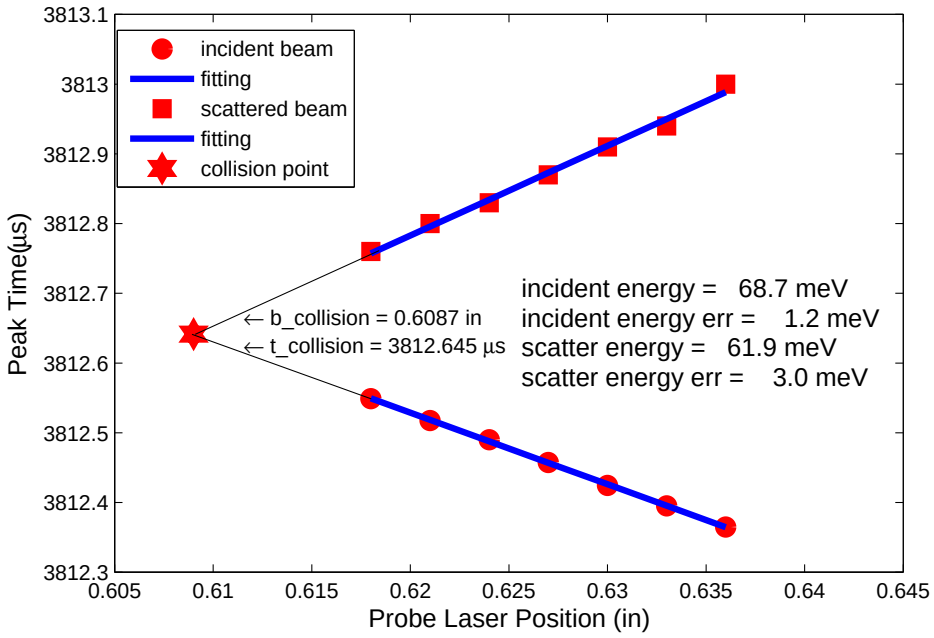

Figure 4.6: Incident and scattered peak times versus probe laser (horizontal) position. The inverse slope of the fittings is used to determine incident and scattered molecules' mean translational velocities as well as to find the surface position and peak arrival time of pumped molecules beam on the surface.

Since the temperature range is high in the cycle of sample heating and measurement, thermal expansion of the sample holder is unavoidable, and that causes the position shift of sample surface and results in systematic error. The method to minimize this error is introduced next.

4.1.2 Systematic Error

During each one hour cycle of the experiment, the sample surface was heated to 1300 K for cleaning and cooled down to 160 K to take measurements. Due to continuous small but unavoidable contamination from the residual gases on the surface, we couldn't wait long enough for the whole sample holder to reach thermal equilibrium, especially for the connection rod between manipulator and sample holder. Since the laser focal positions are controlled in the order of 10^{-5} m, small sample surface position shifts during the experiment were a problem. This shift doesn't cause error for incident molecules' KE measurement. For scattered molecules, if the shift has a random pattern during the one-hour experiment, the error can be averaged out in the result, and that doesn't cause trouble. If the shift has a tendency towards one direction as illustrated in Fig. 4.7, the percentage error can be up to 20% to 30% under certain conditions. In Fig. 4.7, only scattered molecular beam TOF's spectra are presented. Eight TOF spectra are measured by translating the probe laser along the molecular beam axis at time t1,t2...t8 respectively. If the surface position doesn't change, the slope of the dotted line passing through the peak times at different position would give the right information of molecules' velocity. In the real world, the surface position may shift continually to the left, and the wrong velocity information would be given by the solid thick line. In the case shown in Fig. 4.7, the molecules appear to be moving slower than

they actually are.[2]

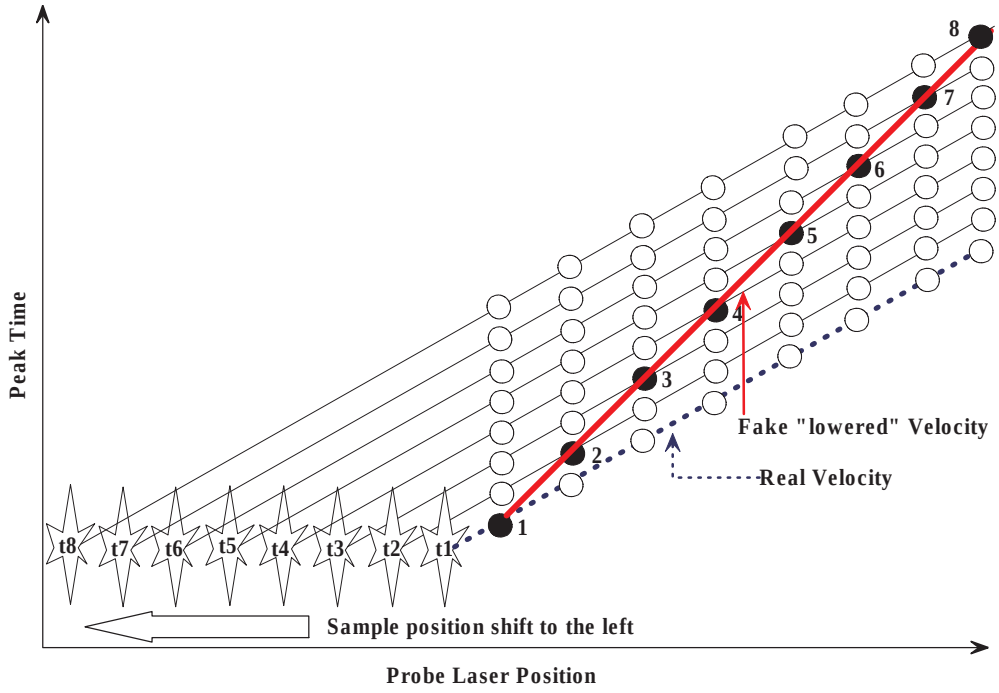

Figure 4.7: Schematic diagram showing the systematic error caused by sample surface position shift under thermal nonequilibrium condition. The dotted line has the right information of the molecules' velocity. The measured velocity from the solid thick line is smaller than it should be in this case.

To minimize this systematic error, a modified experimental procedure was developed. Only two laser positions instead of 8 are used for TOF spectra taken repeatedly, alternately and strictly as shown in Fig. 4.8. Even if the sur-

[2]As indicated above, the source of error is in fact not thermal expansion but thermal nonequilibrium during experiment. The surface position's shift due to the need of studies at different temperature of sample doesn't cause error in velocity/kinetic energy measurement. It is the thermal nonequalibrium of other mechanical parts during experiemnt that causes the troubles.

face position shifts to the left during the whole measurements, the systematic errors average out in the final result. In Fig. 4.8, the linear fitting of "measured" peak times v.s. probe laser positions (solid circles) is parallel to the one under the ideal situation, i.e., no surface position shift. The systematic error is exaggerated as shown in the figures just for presentation. Representative experimental data are shown in Fig. 4.9.

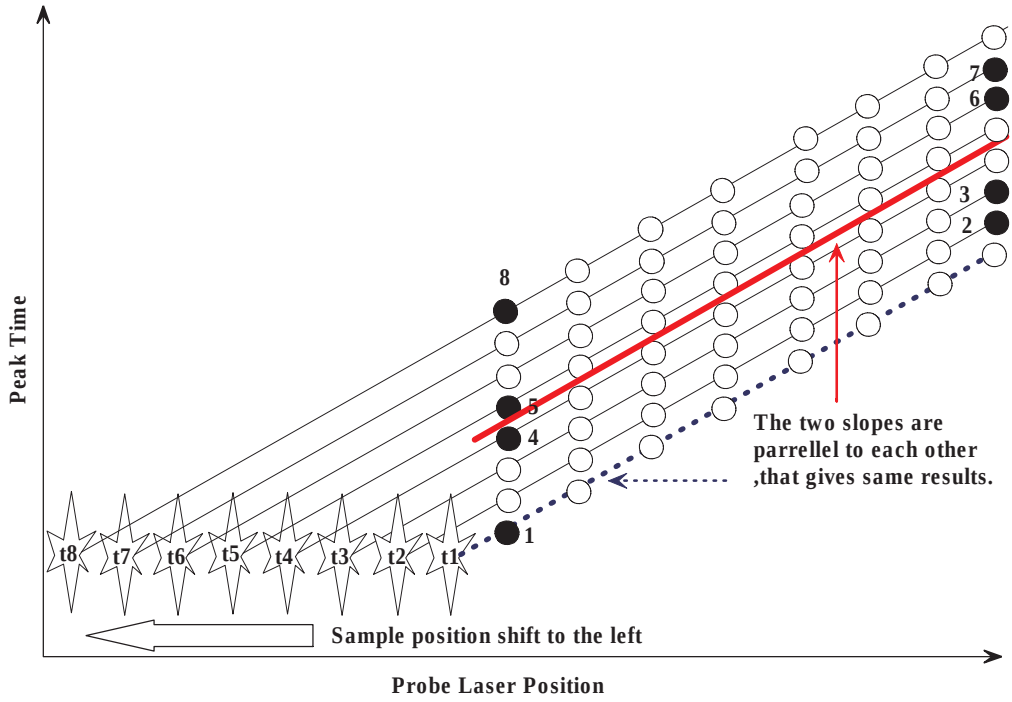

Figure 4.8: Schematic diagram showing the modified experimental procedure to minimize the systematic error. TOF spectra are measured at two probe laser positions (far point and near point) repeatedly, alternately and strictly in the sequence: near, far, far, near, near, far, far, near.

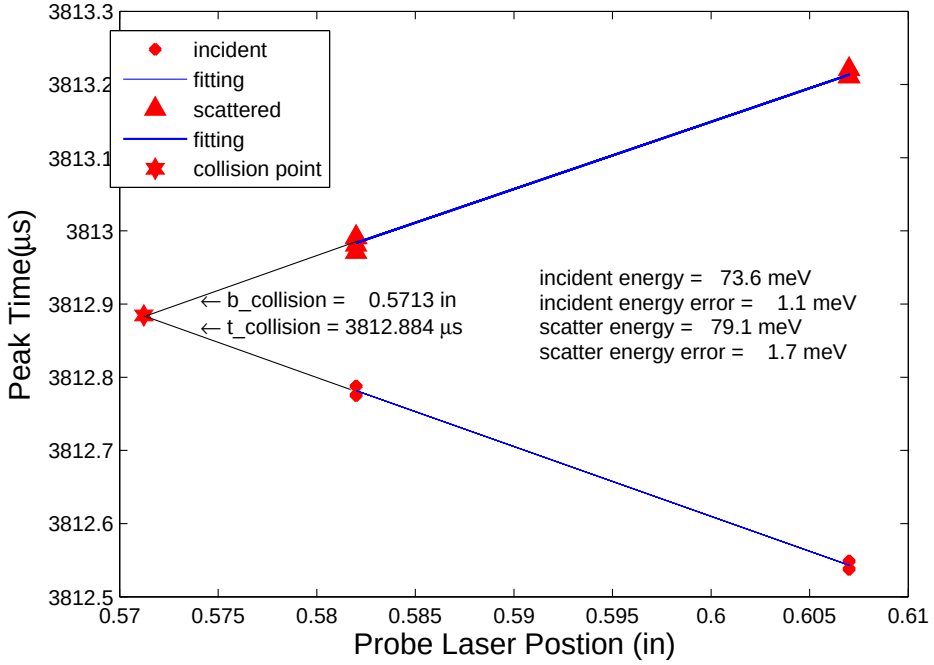

Figure 4.9: Typical measurement of incident and scattered molecules' peak times versus probe laser position in pump/probe TOF experiments. To minimize the systematic error caused by thermal nonequilibrium, the TOF spectra are taken at two probe laser position repeated followed by the procedure introduced in Fig. 4.8.

4.1.3 Change in translational energy versus Surface Temperature

Measurements of change in the translational energy for scattering of H_2(v=1,j=1) from clean Si(100) surface were done at different surface temperatures ranging from 100 K to 1000 K. In these measurements, the incident beam conditions are kept constant. The small variation in incident molecules' translational energies originate from the small changes in the nozzle's working conditions naturally, such as nozzle temperature and gas pressure etc. The results of these measurements are shown in table 4.1, which is also plotted in Fig. 4.10. A mean translational energy loss was found previously for the studies of H_2/D_2 on Cu [49][23] [55], in which the energy loss to the substrate was explained using the classical Baule equation [3][62] and quantum electron friction effect[53] [36].[4] In the case of H_2/Si system, we observed a surface temperature dependence of mean translational energy change. At low surface temperature, the mean translational energy of scattered molecules is lower than that of incident molecules, by contrast, at high surface temperature, the mean translational energy of scattered molecules is higher than that of incident molecules as shown in Fig. 4.10. This can't be explained using the theories for H_2/Cu or D_2/Cu. We will go back to this discussion after more information is presented.

[3]The equation $\Delta(T_S) \cong \frac{4\mu}{(1+\mu)^2}[E_i - \frac{1}{2}k_B T_S]$ where Δ is the change in energy, μ is the mass ratio $M_{H_2/D_2}/M_{Cu} = 0.032/0.065$,$T_S$ is the surface temperature,E_i is the kinetic energy of the incident molecules,k_B is the Boltzmann constant.

[4]In this model, the incident kinetic energy is used to excite electron-hole pairs in the metal. It is a non-adiabatic process.

Table 4.1: Change in translational energy for scattering of H_2(v=1,j=1) from clean Si(100) at different temperature of sample.

Temperature(K)	Incident Energy(meV)	Scattered Energy(meV)
106	68.7 ± 1.2	61.9 ± 2.2
109	71.6 ± 1.6	61.9 ± 1.7
119	76.8 ± 1.0	70.7 ± 2.3
150	75.3 ± 1.1	74.2 ± 5.4
200	72.1 ± 1.1	71.1 ± 3.0
250	76.7 ± 2.1	79.1 ± 3.1
300	75.4 ± 1.4	75.3 ± 3.5
350	75.4 ± 1.5	80.5 ± 5.1
400	73.6 ± 1.7	79.1 ± 5.5
450	74.6 ± 1.5	82.7 ± 8.1
550	74.6 ± 1.2	81.1 ± 7.9
650	73.4 ± 1.1	86.5 ± 13.1
700	72.5 ± 1.4	82.7 ± 10.2
750	73.7 ± 1.1	90.1 ± 16.8
750	73.0 ± 1.2	85.8 ± 12.8
800	77.3 ± 1.0	88.5 ± 11.1
850	73.1 ± 1.2	94.9 ± 21.9
900	77.3 ± 1.1	90.6 ± 13.3
924	75.5 ± 1.0	82.5 ± 6.9
944	76.1 ± 1.2	94.9 ± 18.8
962	72.0 ± 1.7	82.7 ± 10.7
973	76.7 ± 1.3	94.9 ± 18.2

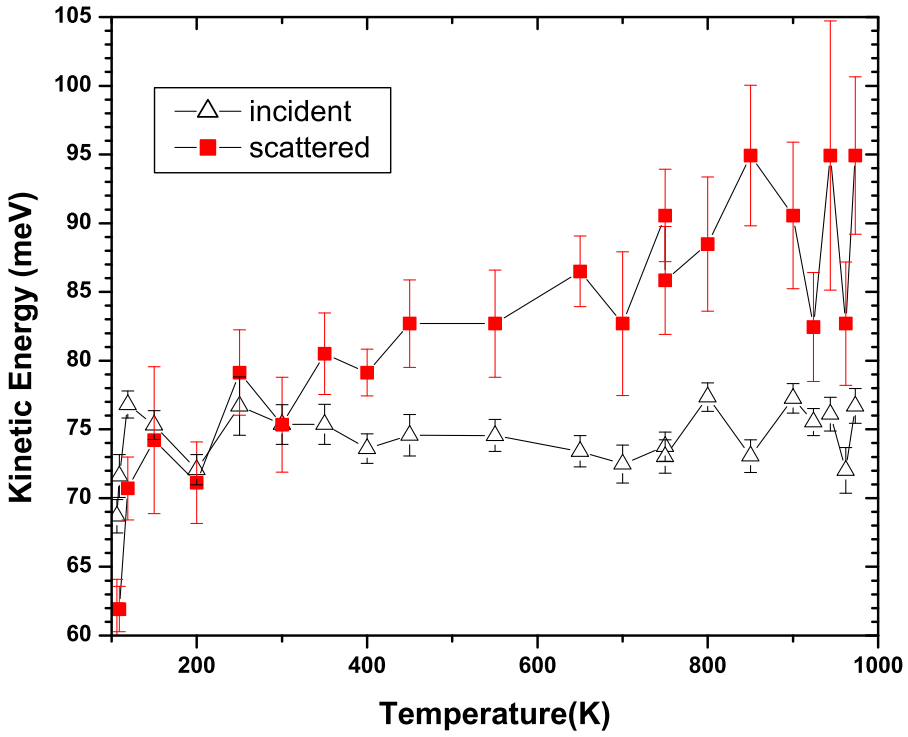

Figure 4.10: Change in translational energy for scattering of H_2(v=1,j=1) from clean Si(100) at different temperature of sample.

4.2 Absolute Survival Probability

4.2.1 Measurements and Data Processes

The change in translational energies shows strong variation with surface temperature. How about the survival probability for different surface temperatures? To measure the absolute survival probability of H_2(v=1,j=1), TOF scans are taken with the probe laser at different vertical positions as shown in Fig. 4.11. There are two ways to calculate the total number of molecules in a beam pulse: integrating the density of molecules over space or integrating the flux of molecules over time. The relationship between density and flux is simple:$flux = density \times velocity$. Note: REMPI signal is in fact a measurement of the density of molecules at the point where the probe laser passes through the molecular beam while the TOF spectra is collection of REMPI signals by scanning in time. Direct integrals of TOF spectra don't give the correct results. Taken above analysis into consideration, each TOF spectrum must be transformed from a density-weighted spectrum to a flux-weighted spectrum. The transformation is discussed in Appendix B. A 3D graph and a contour map for the same data set are present in Figures 4.12 and 4.13 respectively. The distance between sample surface and probe laser in this measurement is 0.0125 in. In Fig. 4.12 the solid line between incident and scattered molecular pulse represents the peak arrival time when molecules hit the surface.

The integrals over time under the incident and scattered peaks in the flux weighted spectra were computed for each TOF scan. Figure 4.14 shows the integrals versus the probe laser vertical position. Gaussian fitting is used

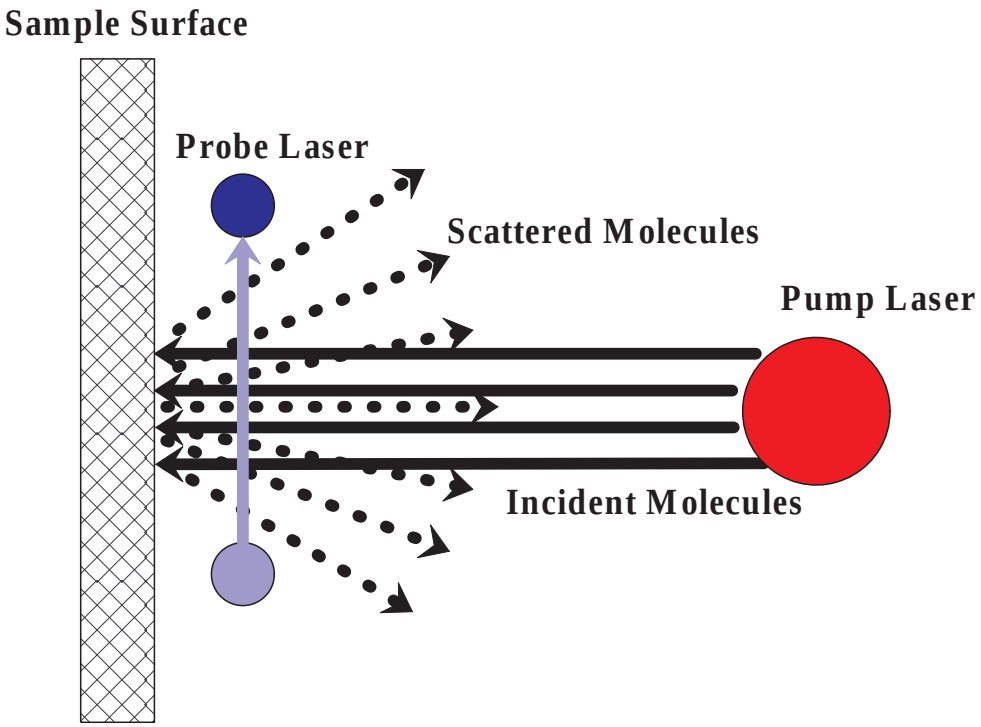

Figure 4.11: Schematic Diagram of measuring the survival probability.

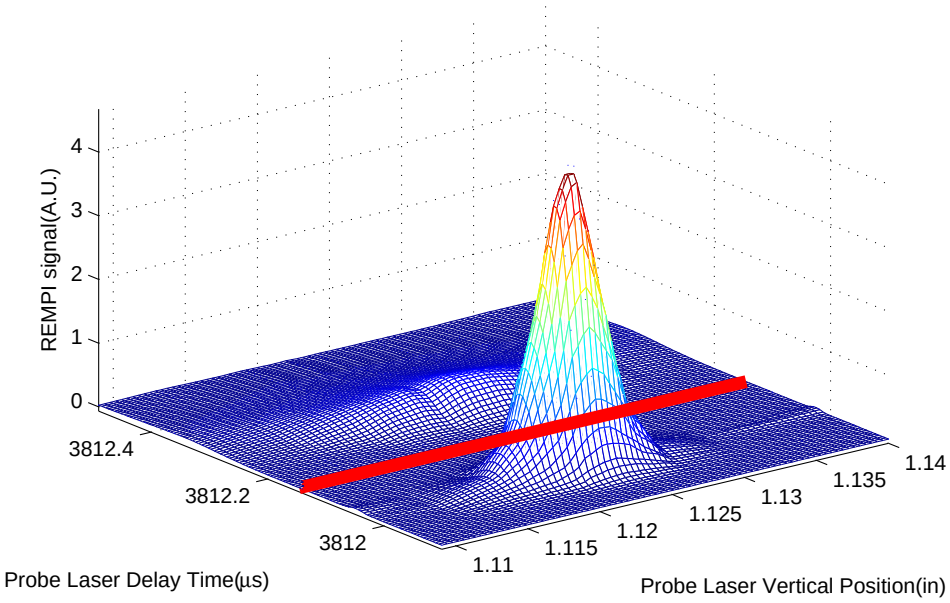

Figure 4.12: 3D visualization of the experimental data (flux-weighted) in the measurement of absolute survival probability.

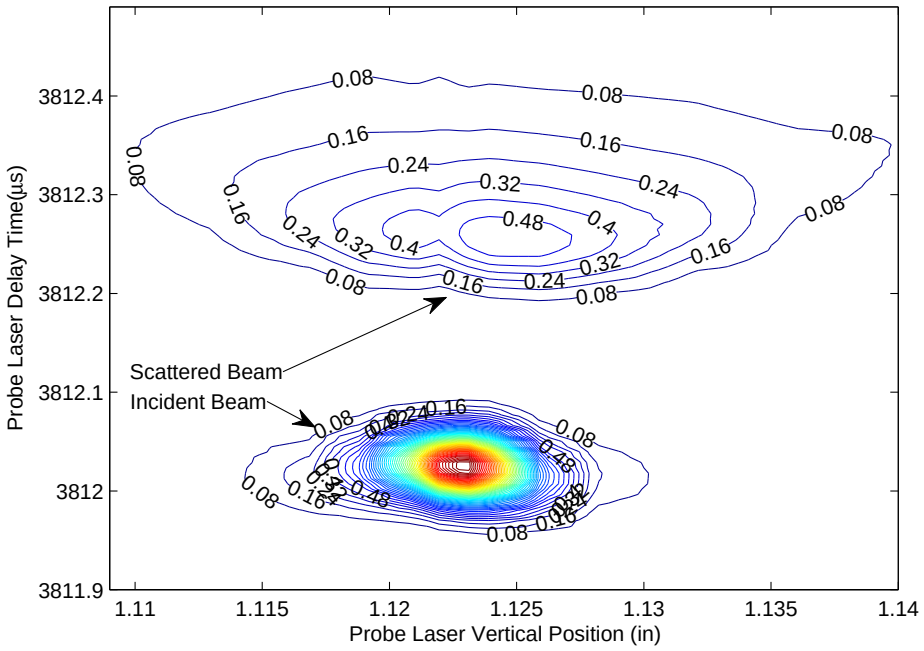

Figure 4.13: A contour map of the experimental data (flux-weighted) as shown in Fig. 4.12.

to fit both the incident and scattered profiles and the ratio of the area under each curve gives the absolute survival probability of H_2(v=1,j=1) scattered from clean Si(100). The spatial profile of the scattered molecules is broader than that of the incident. A study of the angular distribution of scattered molecules will be discussed in Chapter 5 using a fitting model involving Monte Carlo simulation.

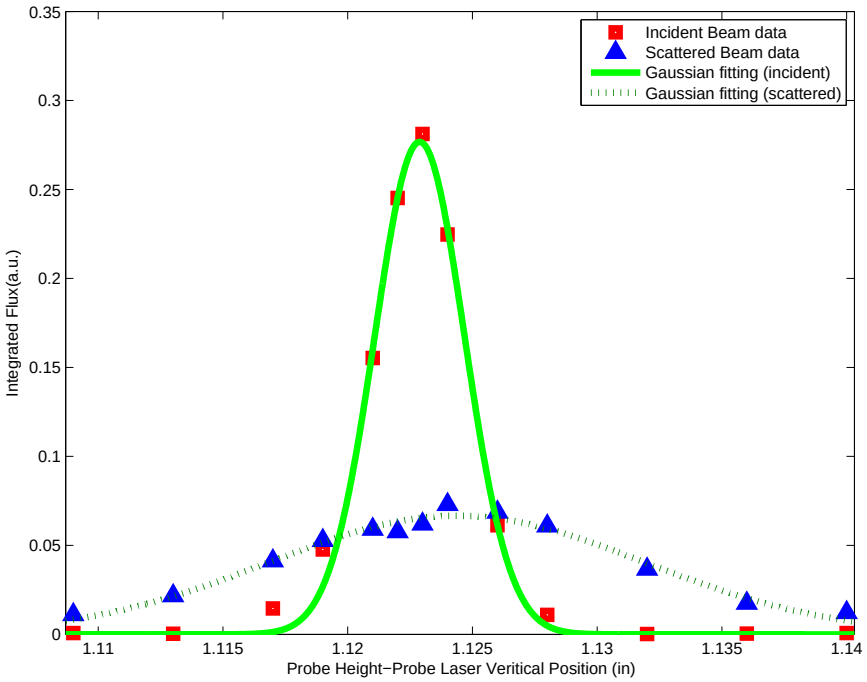

Figure 4.14: Spatial profile of incident and scattered H_2(v=1,j=1) flux from clean Si(100) probed at distance of 0.015 in to the surface. The ratio of the area under the Gaussian fitting curves gives the absolute survival probability. Same data set as shown in Fig. 4.12.

4.2.2 Absolute Survival Probability versus Surface Temperature

The absolute survival probabilities were measured at two extreme temperatures, low at 110 K and high at 973 K. It was found to be close to 1 within uncertainty both at low and high temperature. Experimental data are shown in Table 4.2 and plotted in Fig. 4.15. The incident molecules's translational energy was fixed at 74.3 ± 2.2 meV. Gostain measured the survival probability of H_2(v=1,j=1) from Cu(110) versus incident energy. When incident energy is 77 meV, the survival probability is found to be 0.67 ± 0.09 [15]. It was concluded that one third of incident molecules were lost in three possible channels: rotational excitation within the v=1 manifold, i.e.(v=1,j=1→3); vibrational relaxation to any odd J state in the ground state v=0 manifold; or dissociation (sticking) on the surface. In the case of H_2/Si, we could't find a H_2(v=1,j=3) signal and an upper limit equal to 2% for the probability of rotational excitation (v=1,j=1→3) was given by estimating the system detection limit. The probability of dissociation is extremely low as discussed in Chapter 1. The absolute survival probability of approximately one shows that the probability of vibrational relaxation to any odd J state in the ground state v=0 is small also. Most of the incident molecules are scattered without any internal quantum state transition, i.e. elastically, under current measurement condition.

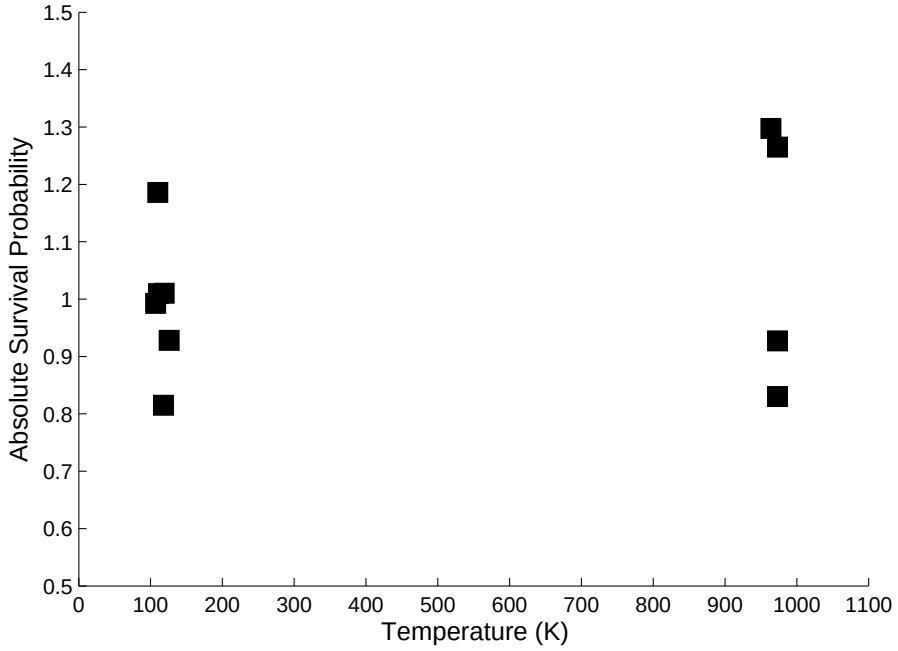

Figure 4.15: Absolute Survival Probability Measurements at low surface temperature (110K) and high surface temperature(973K). Results are averaged and used to calculate the uncertainty.

Table 4.2: Absolute Survival Probability Measurement at low(110k) and high(973K) temperature.

Temperature	Absolute Survival Probability	Mean	Uncertainty
low(110K)	0.81 0.81 1.01 0.93 1.26 0.99 0.93	0.99	0.15
high(973K)	1.19 1.30 0.83 1.0	1.08	0.20

Chapter 5

Elastic Scattering of H_2(v=0, j=1) from Si

As introduced previously, there is an uncertainty in the surface position that results from thermal nonequilibrium. The shift will make it difficult to look into the TOF profile of scattered H_2(v=1,j=1) molecules to extract more information other than mean translational energy and survival probability, since the profile itself is very sensitive to the sample surface position. When scattering of H_2(v=0,j=1) is studied, the ground state scattered molecules are probed after they are scattered back and pumped/excited by pump laser. The TOF profile is not defined by sample surface position but by the pump laser position, which is considered well defined. The thermal shift won't cause any inaccuracy during measurements. In this chapter, a new numerical method based on Monte Carlo simulation is developed. In addition to the change of scattered molecules mean translational energy, more kinetic information, such as angular and velocity distributions are extracted from the experiments.

5.1 Monte Carlo Simulation Based Parameter Optimization Method

The kinematics for the scattered molecules H_2(v=0, j=1) from clean Si surface was simulated using a Monte Carlo method which included several

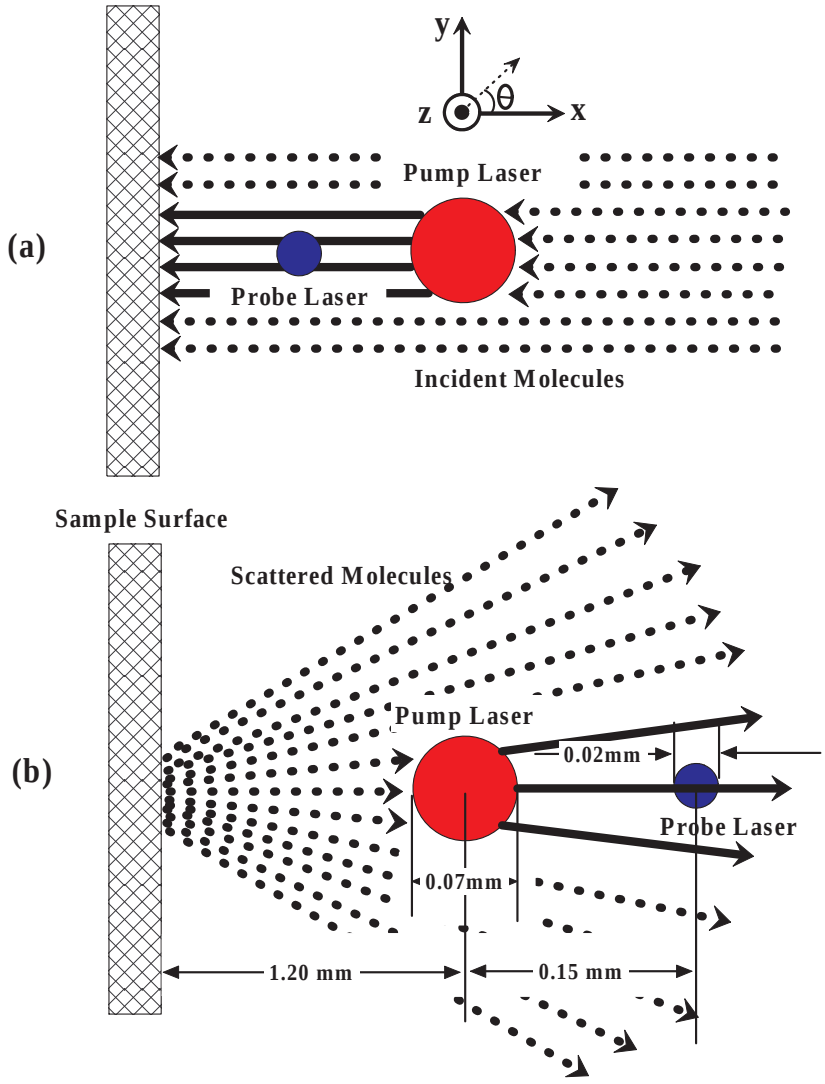

Figure 5.1: Schematic Diagram of $H_2(v = 0, j = 1)$ scattering experiment. The pump laser position is fixed. The probe laser position is changed depending on which molecules (incident/scattered) are studied. Molecules in ground state (v=0,j=1)(solid line) and in excited state(v=1,j=1)(dotted line) are also demonstrated in figure. The coordinate systems are defined as shown.

model parameters. We have chosen simple but physically reasonable forms for these parameters in the absence of more detailed knowledge. These parameters are optimized using non-linear least square method to best fit the experimental data.

We follow the Monte Carlo simulation routine:[45]

1. Monte Carlo Simulation Model.

   A focused Pump laser with a circular cross-sectional Gaussian intensity profile is used to pump ground state H_2(v=0,j=1) molecules to excited H_2(v=1,j=1). The experiment setups are shown in Fig. 5.1 for studies of incident and scattered molecules respectively. In both scenarios, the pumped/excited molecules are initially confined in the pump laser volume. The pumped molecules spatial density is even distributed along the pump laser and has the same Gaussian-like cross-section as the pump laser:

$$P(x) = \frac{1}{\sqrt{2\pi\sigma_x^2}} e^{-\frac{(x-x_{pump})^2}{2\sigma_x^2}} \tag{5.1}$$

$$P(y) = \frac{1}{\sqrt{2\pi\sigma_y^2}} e^{-\frac{(y-y_{pump})^2}{2\sigma_y^2}} \tag{5.2}$$

$$P(z) = 1/L_{pump} \tag{5.3}$$

   where x_{pump}/y_{pump} are the x/y coordinates of the pump laser center position, σ_y/σ_x is the x/y position variance (the measure of the width of

the distribution), and L_{pump} is the pump laser effective length, which is in fact defined by the Si sample size.

For incident molecules the supersonic beam has a very narrow angular distribution towards the sample and speed distribution. For scattered molecules, the angular distribution is represented by a cosine-like distribution. The nature of this distribution is occasionally misinterpreted as $\cos^n(\theta)$[16]. Remember that in the system of spherical polar coordinates the solid angle is given by $d\omega = \sin(\theta)d\theta d\varphi$. So

$$P(\theta) \propto \cos^n(\theta)\sin(\theta) \tag{5.4}$$

$$P(\varphi) = 1/2\pi \tag{5.5}$$

where θ is polar angle and φ is azimuth angle. The speed distribution is represented by a shifted Gaussian distribution:

$$P(v_s) = \frac{1}{\sqrt{2\pi\sigma_v^2}} e^{-\frac{(v_s-\overline{v_s})^2}{2\sigma_{v_s}^2}} \tag{5.6}$$

where $\overline{v_s}$ is th scattered molecules mean translational speed, and σ_{v_s} is the speed variance.

The probe laser is considered less complicated than pump laser due to its smaller focus size compared with pump laser's. The detection volume is modeled as a cylinder. Any molecule entering this cylinder when the probe laser is fired will be ionized and detected by CEMA.

2. Perform a deterministic computation for each molecule.

We are not performing a dynamic simulation but rather pure kinematic simulation, no interaction is modeled. For each molecule, the trajectory is immediately determined by its initial position (x, y, z) and (v_x, v_y, v_z)[1] If the trajectory is intercepted by the probe laser. The molecule will be marked as "detected". Next, create a histogram of times at which the molecule is detected with the same time interval (10 ns) as the experiment.

3. Aggregate the results of the individual computations into the final result.

   Basically the kinetic question is a multidimensional integral with complicated boundary conditions. It is difficult to solve with analytical calculations. Monte Carlo simulation is a straightforward and simple way to solve this kind of integral problem. To get a smooth simulation result (TOF spectrum), 1,000,000 trajectories are aggregated.

4. Optimize the kinetic parameters by non-linear least square method.

   We combine several parameters in the simulation. Some parameters are known directly, such as the probe laser firing time, probe laser position and pump laser effective length. Plot the peak times versus probe laser positions, the intersection determines the pump laser position and firing time. Some parameters don't seem to affect the scattered profile, such as the size of probe laser and effective length. We just pick a value for them.

[1] If incident molecules are studied, $v_y = 0$ and $v_z = 0$; if scattered molecules are studied, v_x, v_y, v_z are calculated by $v_x = v\cos(\theta), v_y = v\sin(\theta)\cos(\varphi), v_z = v\sin(\theta)\sin(\varphi)$.

Some parameters are optimized by fitting the incident TOF spectra, such as the size of the pump laser and incident molecular speed. Once all parameters are obtained, the scattered molecules' angular distribution, scattered mean speed and speed distribution are extracted by fitting the scattered TOF spectra. Sample fitting results based on Monte Carlo Simulation are shown in Fig. 5.2. The extracted kinetic parameters will be given next section.

5.2 Results-Angular and Velocity Distributions, Mean KE versus Surface Temperature

We noticed that the TOF spectra varied with surface temperature. This is shown in Fig. 5.3.[2] Sample TOF spectra at three different temperatures are scaled to the maximum value[3]. The solid curves are fits to the experimental TOF data introduced in the last section. At higher surface temperature, the peak time is shifted to a slightly earlier time and the profile becomes markedly narrower. These phenomena can be explained clearly when the kinetic parameters are extracted from the fitting. The results are shown in Fig. 5.4 – 5.9. The data are shown in Table 5.1 and 5.1 for scattered and incident molecules respectively.

[2]While H_2(v=0,j=1) is studied, Sample position doesn't have effect on the measurement of TOF spectra. The pump laser position is calibrated the same way as we study H_2(v=1, j=1) to find the sample position by changing the probe laser position along the molecular beam axis. In stead of sample position, the pump laser position as well as pump time is

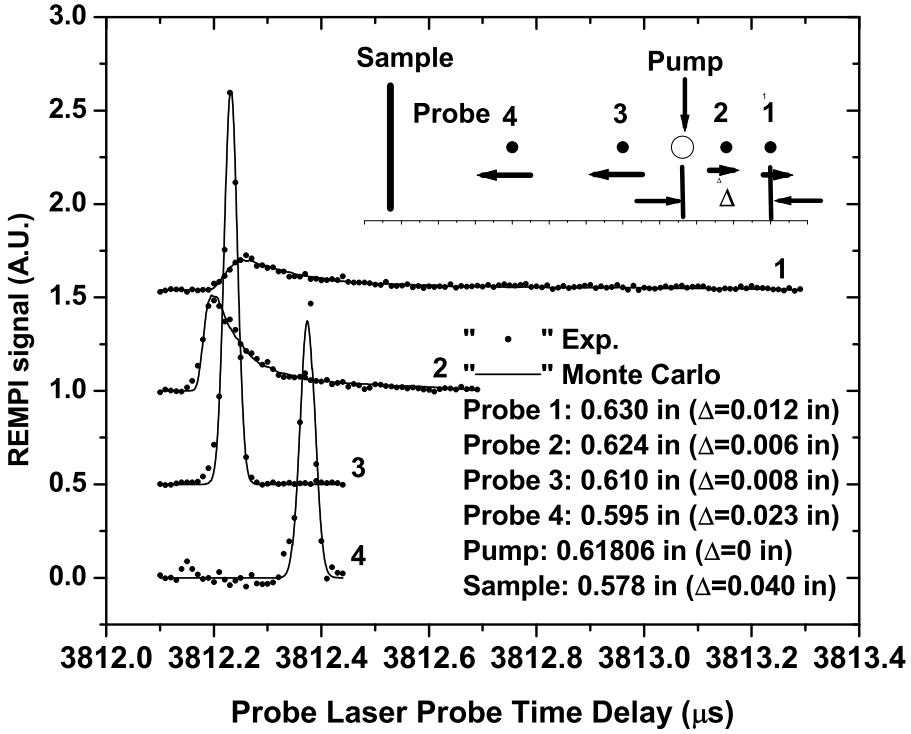

Figure 5.2: Sample fitting results based on Monte Carlo Simulation. The TOF spectra are measured at various probe laser position as shown in the insert. The experimental data are well fitted for both incident and scattered molecules.

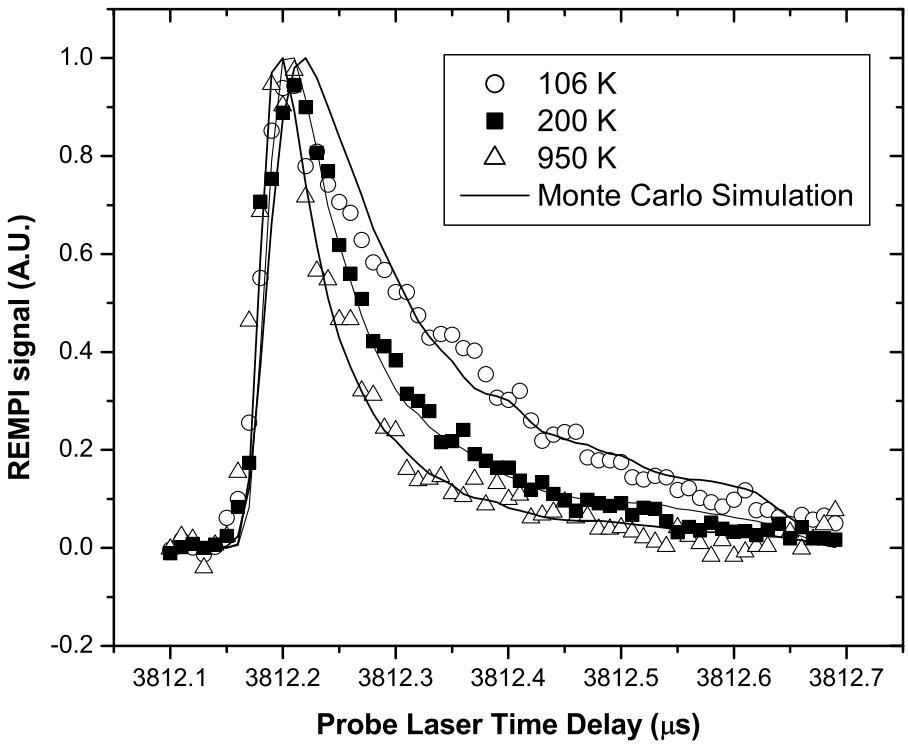

Figure 5.3: Sample TOF spectra at 3 different surface temperature. Pump laser position: 0.6181 in and probe laser position:0.6240 in. Sample postion: 0.578 in. The three spectra are scaled to the same maximum. The TOF profiles shows a different pattern.

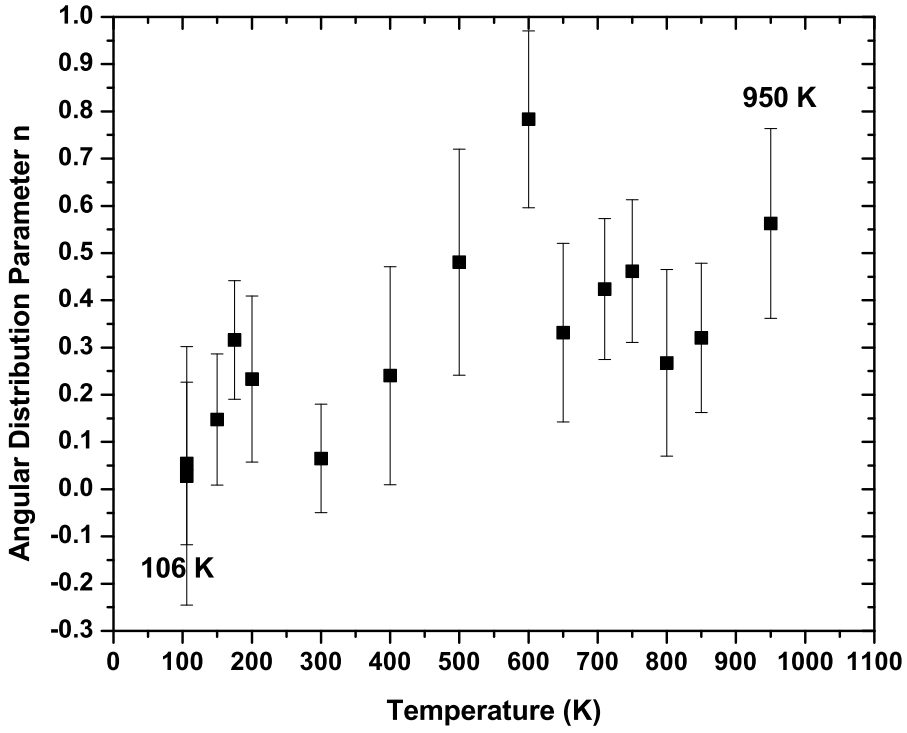

Figure 5.4: Scattered Molecules' angular distribution parameter n versus surface temperature.

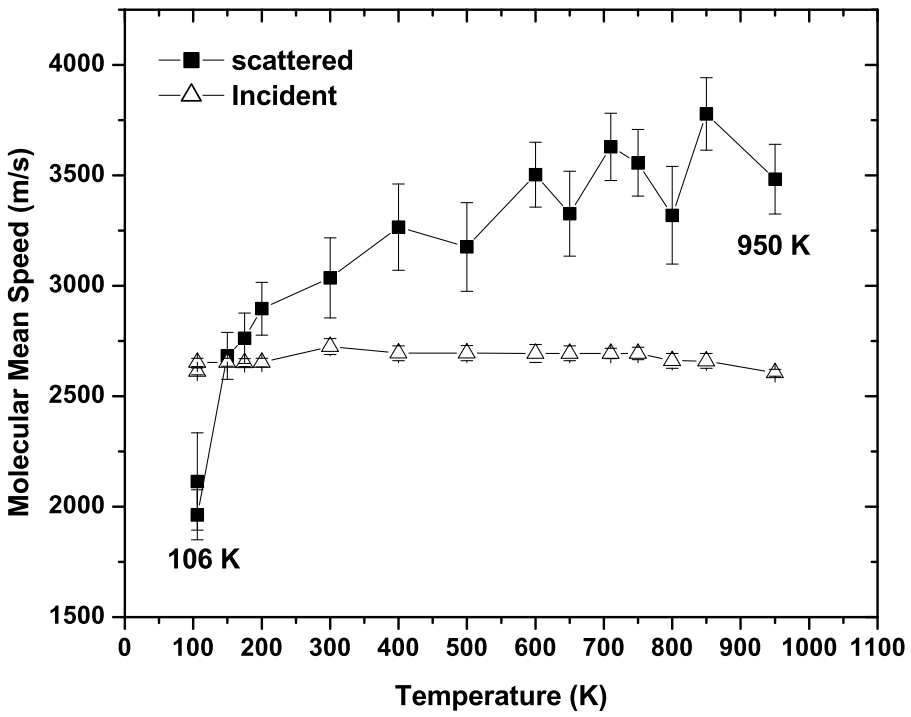

Figure 5.5: Scattered Molecules' mean speed versus surface temperature. Incident molecules' speed is obtained similarly by MC fitting.

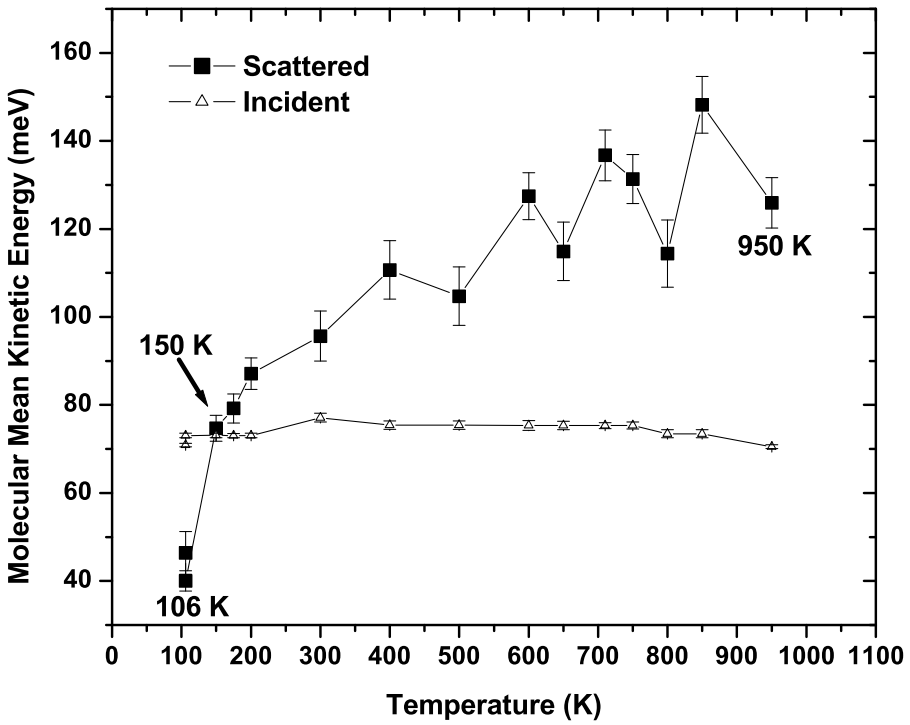

Figure 5.6: Same results from Fig. 5.5. Conversion from speed to KE.

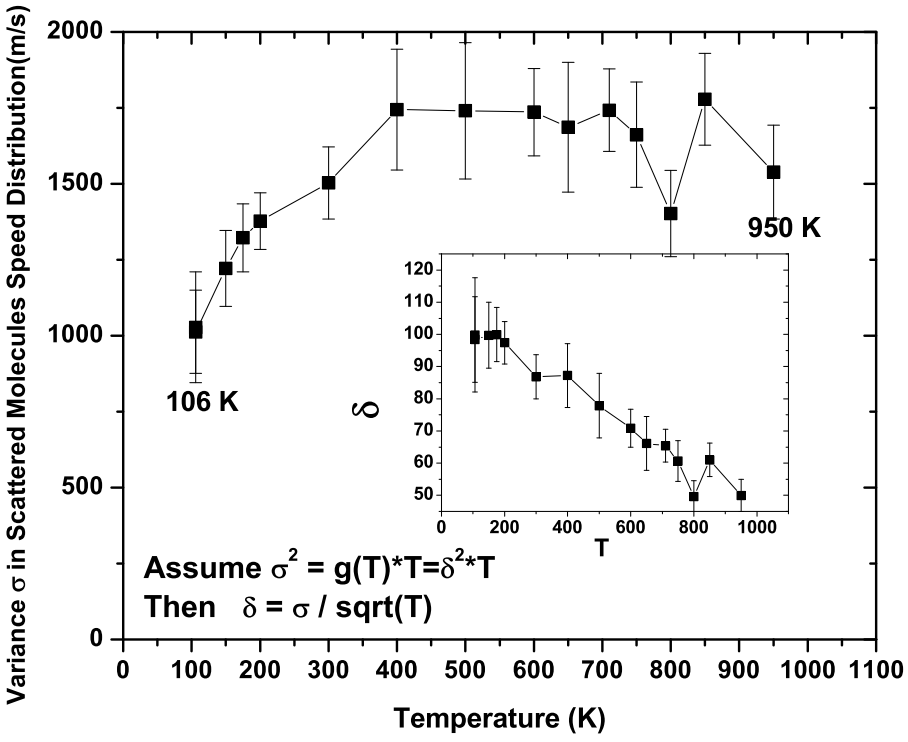

Figure 5.7: Scattered Molecules' speed distribution parameter σ_{v_s} versus surface temperature.

Table 5.1: Scattered Molecules' kinetic parameters at different surface temperatures.

T(K)	n	Δn	$\overline{v}(m/s)$	$\Delta\overline{v}$	$\overline{KE}(meV)$	$\Delta\overline{KE}$	$\sigma_v(m/s)$	$\Delta\sigma_v$
106	0.03	0.27	2113	220	46.3	4.8	1027	182
106	0.05	0.17	1962	113	40.0	2.3	1012	136
150	0.14	0.14	2682	106	74.7	3.0	1221	124
175	0.32	0.13	2762	114	79.2	3.2	1322	124
200	0.23	0.17	2897	119	87.1	3.6	1377	93
300	0.07	0.11	3035	181	95.6	5.7	1503	118
400	0.24	0.23	3265	196	110.7	6.6	1744	199
500	0.48	0.23	3176	200	104.7	6.6	1741	225
600	0.78	0.19	3503	146	127	5.3	1736	144
650	0.33	0.19	3327	192	115	6.6	1687	214
710	0.42	0.15	3629	153	137	5.8	1743	136
750	0.46	0.15	3557	151	131	5.6	1662	173
800	0.26	0.19	3319	221	114.4	7.6	1402	141
850	0.32	0.16	3778	164	148.1	6.4	1779	151
950	0.56	0.20	3482	158	125.9	5.7	1538	154

Table 5.2: Incident Molecules' kinetic parameters at different surface temperatures.

T(K)	$\overline{v}(m/s)$	$\Delta\overline{v}$	$\overline{KE}(meV)$	$\Delta\overline{KE}$
106	2613	16	70.9	0.4
106	2652	19	73.0	0.5
150	2653	18	73.1	0.5
175	2652	19	73.0	0.5
200	2653	19	73.0	0.5
300	2725	36	77.1	1.0
400	2695	34	75.4	0.9
500	2695	40	75.4	1.0
600	2693	40	75.3	1.1
650	2694	33	75.4	0.9
710	2693	23	75.3	0.8
750	2693	28	75.3	0.8
800	2660	34	73.5	0.9
850	2660	34	73.5	0.9
950	2606	16	70.5	0.4

Note that[4]:

1. T: surface temperature;
2. n: scattered molecules' angular distribution parameter;
3. Δn: uncertainty of scattered molecules' angular distribution parameter;
4. $\overline{v}$: molecular mean speed;
5. $\Delta\overline{v}$: uncertainty of mean speed;
6. $\overline{KE}$: molecular mean kinetic energy;
7. $\Delta\overline{KE}$: uncertainty of molecular mean kinetic energy;
8. σ_v: scattered molecules' speed distribution parameter;
9. $\Delta\sigma_v$: uncertainty of scattered molecules' speed distribution parameter;

5.3 Discussion

Not surprisingly, the ground state H_2(v=0,j=1) has a similar pattern as excited H_2(v=1,j=1) for the mean translational energy change versus surface temperature. The difference is that H_2(v=0,j=1) molecules gain more

given by the intersection of incident and scattered lines.

[3]The amplitude of TOF signal is sensitive to laser power which is not well monitored. It is difficult to compare the amplitude by itself.

[4]Kinetic Parameters are defined in last section. The uncertainties are calculated from fitting results with 95% confidence intervals statistically.

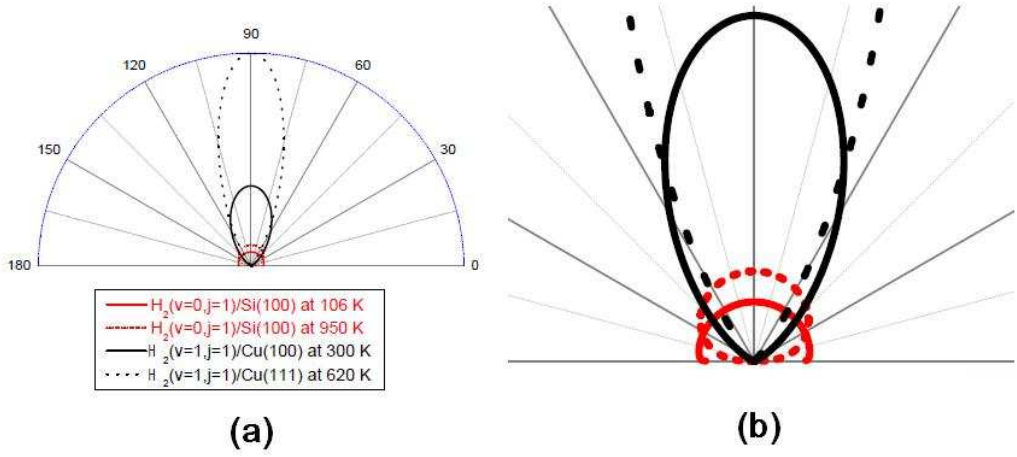

Figure 5.8: Comparison of angular distributions ($\frac{1}{P(n)}\cos^n\theta$). Original data of H_2/Cu system are from Gostein [13]. All data are normalized to make $\frac{1}{P(n)}\int_0^{\frac{\pi}{2}}\int_0^{2\pi}\cos^n\theta\sin\theta\,d\theta\,d\varphi = 1$, where $P(n)$ is normalizing constant.

energy from the substrate at high temperature than H_2(v=1,j=1). For both kinds of molecules, there exists a critical surface temperature (around 180 K for H_2(v=0,j=1),roughly 200 K for H_2(v=1,j=1)), below which the mean KE of scattered molecules is lower than that of incident molecules. Above that temperature, the mean KE of scattered molecules is higher than that of incident molecules and the change of mean KE gets larger when the surface temperature is increased further.

The angular distribution parameter n versus surface temperature shows a weak surface dependence. More importantly we found a much broader angu-

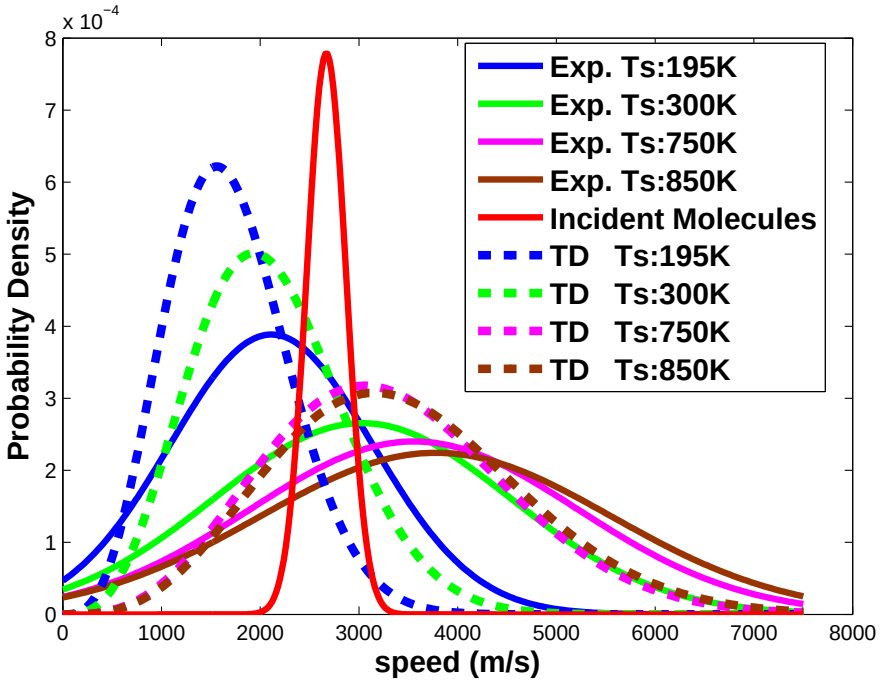

Figure 5.9: Scattered molecules' speed distributions at various surface temperatures. The red line shows the incident molecules' speed. All data are normalized to make $\int_0^\infty P(v)\,dv = 1$ except that for incident molecules. Solid line: experimental data; dotted line: results from trapping-desorption.

lar distribution than one described by Knudson cosine law[5]. The typical value of "n" is changing from 0.04 ± 0.22 at 106 K to 0.56 ± 0.20 at 950 K. This is very different from the results of H_2/Cu system. Gostein's works showed that n is 6.5 ± 0.8 at 90 K, 5 ± 1 at 300 K, 15 ± 5 at 620 K for H_2(v=1,j=1)/Cu(110) system, and 18 ± 6 at 90K, 15 ± 6 at 620 K for H_2(v=1,j=1)/Cu(111) system. The angular distributions of the scattered H_2 from clean Si at different surface temperatures are shown in Fig. 5.8, which are compared with the results of H_2/Cu from Gostein. The reason is that metal surface has a more "flat" and dense surface that Si surface. Because of localized covalent bond, Si surface are generally reconstructed, therefore corrugated. The impinging molecules on the corrugated surface exhibit a broader scattering angle than on metal surfaces.

The third kinetic parameter extracted from the Monte Carlo simulation based fitting is the width, i.e. speed variance σ_v of speed distribution. σ_v increases with surface temperature up to 400 K and approaches a limit. More interestingly if we think that σ_v is a function of surface temperature in the form of $\sigma_v = \delta^2 T_s$, the transformed factor δ has a linear dependence on surface temperature[6].

Considering one type of limiting collisions: trapping-desorption scattering (TD), all of the scattered molecules are accommodated with the surface,

[5]A law which states that the probability for a gas molecule to leave a solid surface in a given direction within a solid angle $d\omega$ is proportional to $\cos\theta d\omega$, where θ is the angle between the direction and the normal to the surface.

[6]δ is a factor we defined, which has a linear relationship with surface temperature

i.e., the translational temperature of the scattered molecules becomes equal to the surface temperature. The speed distribution of TD scattered molecules is

$$P(v_s) \sim v_s^3 \, e^{-\frac{m*v_s^2}{2*k_b*T_s}}.$$

By comparing our experimental data with the TD results as shown in Fig 5.9, we find that there are significant TD component in the speed distribution of scattered H_2 from Si , but it is still unknown that a trapping desorption intermediate is really involved in the H_2/Si system.

Chapter 6

Conclusion

6.1 Summary

Surface Temperature effects are known to be very strong in H_2/Si system. Previous experimental studies [3] by Bratu and Höfer et al.(1996) using optical second-harmonic methods found that the initial sticking coefficient for H_2 on Silicon increases from 10^{-8} at 550 K to 10^{-5} at 1000 K. This is considered to be a "phonon-assisted sticking" effect completely analogous to the well known "vibrational-assisted sticking" of molecules on metal. Theoretical calculations originally reported by Brenig et al.(1994)[5] proposed adding one substrate degree of freedom. But it is not specified clearly. Dürr and Höfer said, "For this reason the model is not expected to predict any details of the reaction dynamics and any quantitative agreement with the experiment is to some extent accidental."(2006)[12]. Brenig and Pehlke also stated, "The details of the reaction mechanism leading to the observed strong increase of sticking coefficients with temperature and coverage are not known."(2008)[7].

In this work, we studied the surface temperature dependence of scattering of H_2 on clean Si(100) surface using pulsed supersonic molecular beam and quantum state-specific detection techniques. Only one incident energy for

the incident molecules around 74 meV was explored to focus on surface temperature effects. Considering that the barrier to dissociative adsorption for H_2/Si system is approximately 600 meV, the reactivity under our experimental conditions is low even for the excited vibrational state[1]. After careful data processing through convolution fitting (density to flux conversion) and a Monte Carlo simulation based fitting method introduced in the text and appendices, quantitative and reliable kinematic parameters were obtained. When we compared the results with that of H_2/Cu system (a classic activated dissociative adsorption model with a similar adsorption barrier as that of H_2/Si), these parameters are quite distinct from each other. These comparisons are listed below:

1. Mean energy change.

   The mean energy for H_2 in both ground (v=0, j=1) and excited states (v=1, j=1) scattered from clean Si(100) showed strong surface temperature dependence and increased with temperature. Energy gain was observed at high temperature (above 150 K for H_2(v=0,j=1) and above 200 K for H_2(v=1, j=1))[2]. This is contrary to the situation in H_2/Cu, in which the H_2 lost energy to the substrate at all sample temperatures.

2. Absolute Survival Probability.

[1]The absolute survival probability of (v=1, j=1) state is approximately equal to 1.

[2]Also we observed different value in energy gain for (v=0, j=1) and (v=1, j=1). The reason is unknown which need further investigation.

No quantum state transition was found for H_2 (v=1, j=1) scattered from clean Si(100) either at low or high temperature. We measured that the absolute survival probability of H_2(v=0,j=1) was close to 100%. We gave an upper limit equal to 2% for the probability of rotational excitation (v=1,j=1→3). In contrast, significant loss up to 40% was observed for H_2/Cu under similar condition (incident energy and surface temperature).

3. Angular Distribution.

   A remarkably broad angular distribution described by $\cos^n(\theta)$ with the parameter n equal to 0.04 ± 0.22 at 106 K and 0.56 ± 0.20 at 950 K for H_2(v=0,j=1) was observed due to Si(100) surface corrugation. n depends on surface temperature weakly. Generally the scattered H_2 from densely packed metal surface is characterized by a sharp specular lobe with n larger than 5 for H_2(v=1,j=1)/Cu(100) system and larger than 15 for H_2(v=1,j=1)/Cu(111) system[13].

4. Speed Distribution.

   The variance in the speed distribution for scattered H_2 (v=0, j=1) increased with temperature up to 400 K and reached a constant value for higher temperature. No solid data on H_2/Cu exist to be compared with.

The scattering of H_2 on Si has been less studied and very few quantitative experimental and theoretical results have been reported. Using an effusive

hydrogen molecular beam and mass spectrometer instead of pulsed supersonic beam and REMPI technique in this work, Bisson and coworkers[1] measured angular distributions of hydrogen molecules scattered from H-terminated Si surface and found an almost cosine like angular distribution. The same result was given by Namiki and coworkers's measurements [54] using D_2. They also found that when surface temperature is high (600 K), the scattered molecules gained some energy from the substrate by the evidence that the translational temperature of the scattered molecules (431 ± 10 K) is higher than incident molecules (300 K) but still less than the surface temperature of 600 K. Their results are in qualitative agreement with ours.

Overall, our results shows that kinematic parameters of H_2 on Si have a strong dependence on surface temperature and exposed a completely different dynamics from H_2/Metal systems. While the elastic scattering process we studied is far from the dissociative adsorption reaction conditions, the dynamics has already included phonon excitation/deexitation of the silicon substrate, a characteristic that is normally not considered for the studies of H_2 on metal surfaces. More careful theoretical treatment and experimental investigation are needed to explore the nature of H_2 on Si surface. We hope that the detailed results from this work can give some hints and tests for the state-of-art theoretical calculations. Understanding the nature of H_2 on Si at elevated surface temperature may provide a cheaper and cleaner way to passivate Si surfaces in Si industry and nano-technology.

6.2 Future work

Note that all our measurements are averaged over the two domains (2x1) and (1x2) distributed on the Si(100) sample used. Most likely, the angular distributions would be different in the two scattering planes parallel and perpendicular to the Si dimer rows due to different corrugation in the two planes. An asymmetric distribution in azimuth angles is expected from a one-domain Si sample surface.

The dissociative adsorption of H_2 on Si(100) is also activated by incident energy. In this work, we focused on the surface temperature effects. The incident molecular KE is kept constantly low. Studies as a function of incident energy as well as surface temperature is a future goal.

When the surface temperature is higher than 1000K, the radiation from the sample holder causes background on the ion collector. This prevents us from conducting studies at surface temperature higher than 1000 K. The radiation from the luminous sample holder is considered to be the troublemaker. A new ion collection strategy is required to bypass this difficulty.

Appendices

Appendix A

H_2 Molecular Beam

The molecules exit a supersonic nozzle pulsed operating at a frequency of 10 Hz. The beam is skimmed and then chopped by a high-speed rotating chopper disk rotating at 300 Hz. The chopper disk has 4 slits in two different sizes shown in Fig. A.1. The reference signal from the LED phototransistor triggers the nozzle firing. Because the openings of these slits are different. Two kinds of length-different beams can be chosen. Figure A.2 shows both long pulse and short pulse through TOF measurements [1] These pulses have a temporal full width at half maximum (FWHM) of 111.5 μm and 7.3 μs for long and short pulse respectively.[2]

We designed a experiment to measure the number of H_2 per pulse by monitoring the pressure change in the main chamber.[3] By fitting a model involving the chamber's volume, response time of the nanoammeter and pumping

[1] No pump laser was involved. Only the probe laser was used. A time-of-flight scan of the entire molecular beam through H_2 ground state Q1 transition is shown.

[2] These results is consistent with a simple calculation given the size of slit opening (0.619 in and 0.034 in) and chopper's radius (2.74 in) and rotation speed (300 cycles/s), which gives the pulse length 119 ± 11 μs and 6.6 ± 0.6 μs respectively.

[3] This measurement was performed using a liquid nitrogen-trapped oil diffusion pump (Later it was replaced with a turbomolecular pump.).

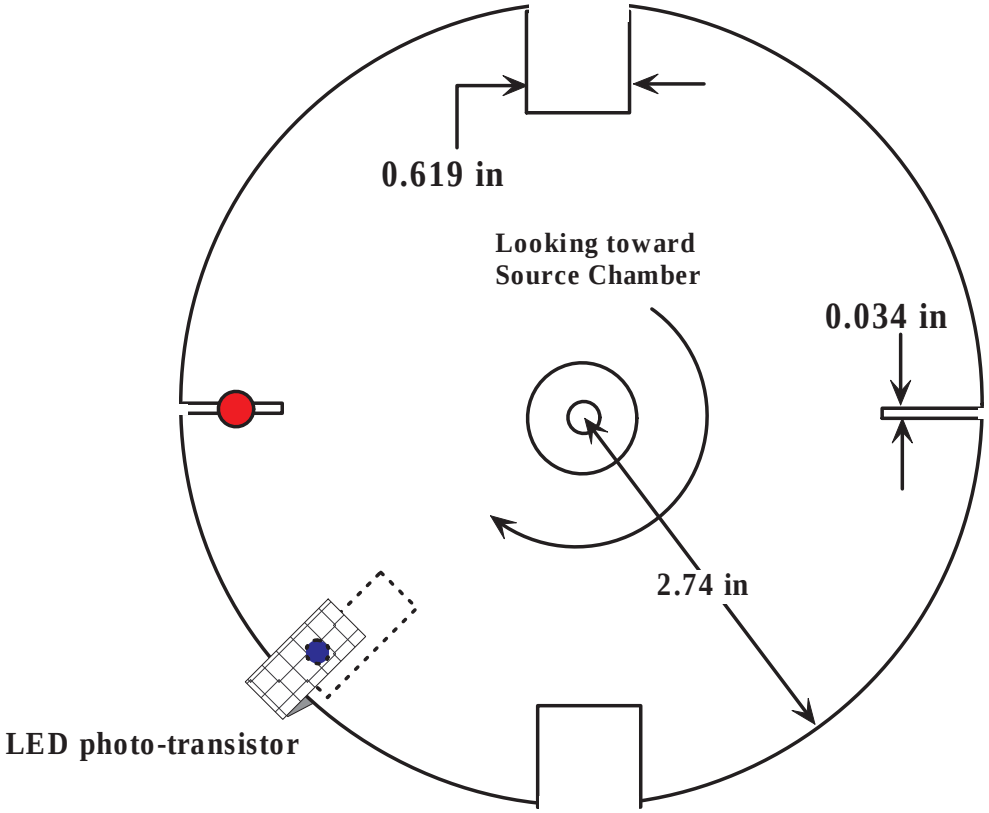

Figure A.1: Schematic diagram of the chopper.

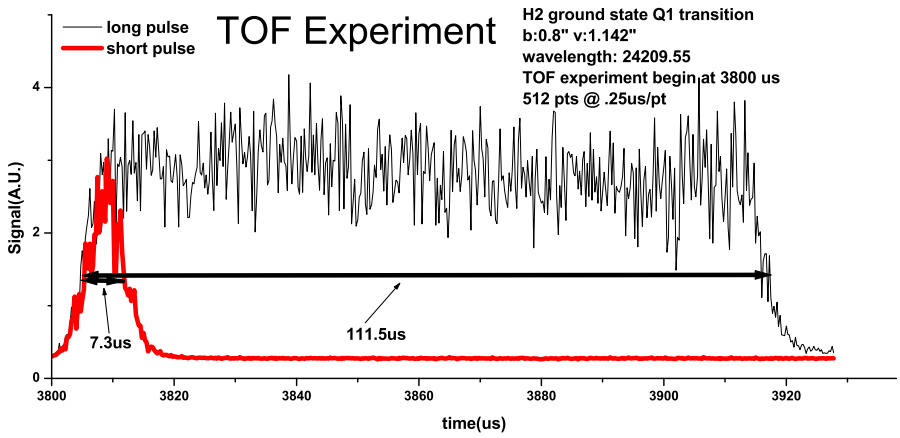

Figure A.2: Comparison of long pulse beam and short pulse beam.

speed[4] as shown in Fig. A.3, we found the flux of the beam source (the nozzle temperature:300 K, H_2 pressure in the nozzle: 20 psi) onto the target is 2.7×10^{13} cm^{-2} (long pulse) and 1.3×10^{12} cm^{-2} (short pluse), corresponding to 0.04 and 0.002 monolayers (ML) per pulse given that Si(100) site density of 0.678×10^{15} cm^{-2}. This long pulse beam is used to quickly build up a saturated layer of hydrogen on the Pd surface. The long pulse wasn't used in Si/H_2 experiment.

We got the short pulse beam density contour map shown in figureA.4 after doing a series of TOF measurements by scanning vertically and converting TOF's time-scanning data into horizontal-position-scanning data by

[4]286.31 L/s was fitting result for the liquid nitrogen-trapped oil diffusion pump.

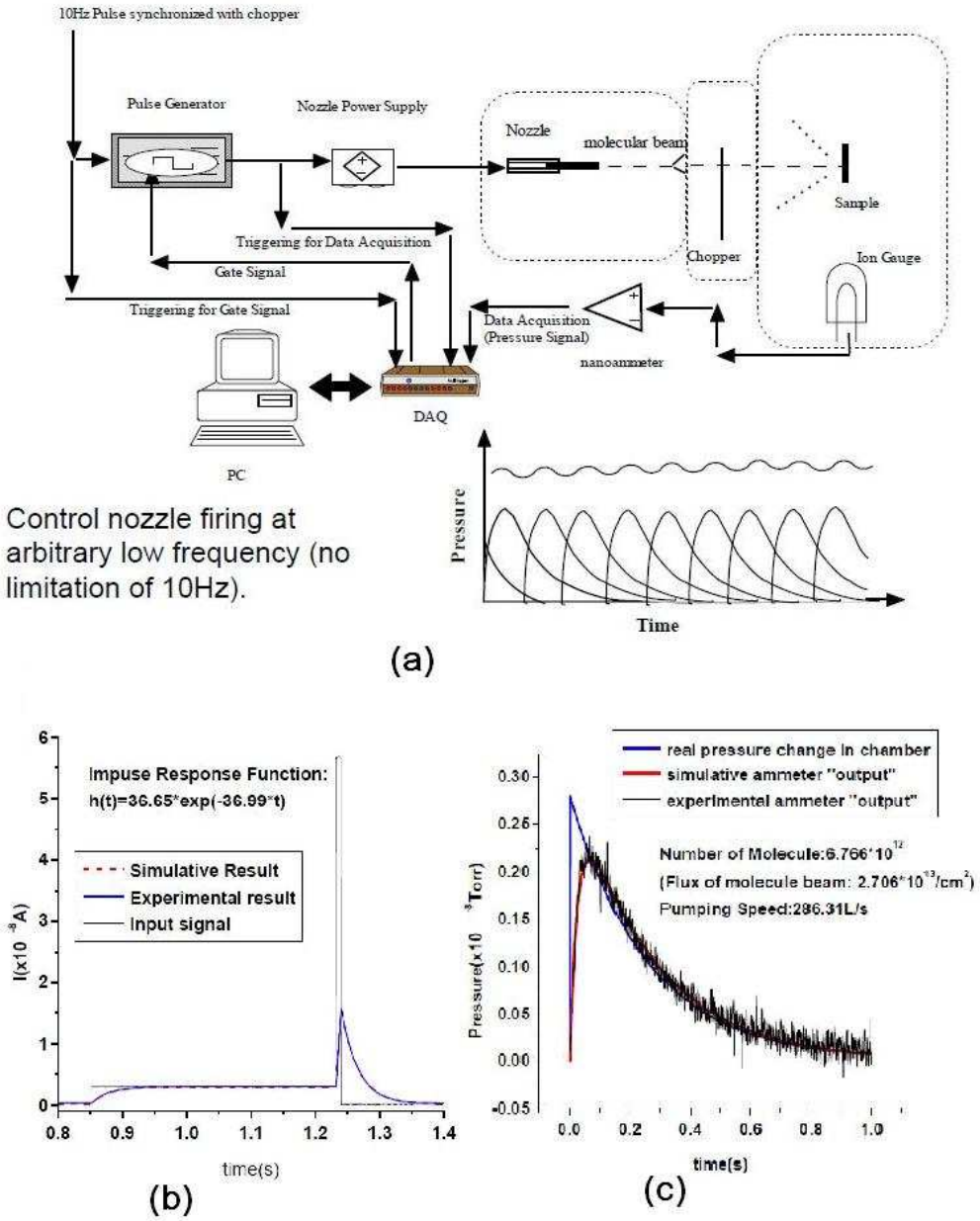

Figure A.3: Experiment to measure the number of H_2 molecules per pulse. (a) experiment set-up. (b)Impulse response function for nanometer. (c) fitting result.

multiplying the time delay with H_2 speed, 2700 m/s. Figure A.4a shows the 1:1 scale side view of the short pulse beam. Figure A.4b is amplified but not in scale. Another vertical scan while the delay time is fixed shows clearly the wire shadow with a width of 0.046 cm in figureA.4c. The reason for a rhombic profile instead of a rectangular one as shown in Fig. A.4b and the unsymmetrical vertical scan profile as shown in Fig. A.4c can be explained by the chopper's cutting through the beam at a limited speed.

Two different size of the chopper's slits results in two kinds of pulses, long pulse and short pulse, in a during of 111.5 $\mu\mu$s and 7.3 μs respectively. The selection is up to the operator. Before the chopper, how long is the beam just after fired from the nozzle and skimmed by the skimmer? The question is answer by scanning the nozzle firing delay time as shown in figureA.5. To do this experiment, the probe laser firing time is fixed, triggered by the only one reference signal from the LED photo-transistor on the chopper, so change of mode won't have any effect on the signal. The only variance is the Nozzle firing delay time. If the nozzle fires too early or too late, the molecular beam will miss the probe laser, resulting no signal. The results shown in Fig. A.5 prove this point and show that the beam pulse before chopper is 248 μs long.

Above measurements are operated with probe laser only through the ground state's Q1 or Q3 transition, this way we look into the whole pulse beam. In most of our experiments, to achieve high time-space resolution, both pump laser and probe laser had to be involved. A typical TOF measurement is shown in Fig. A.6. The time scale (54 ns) of the pumped molecules in Fig. A.6

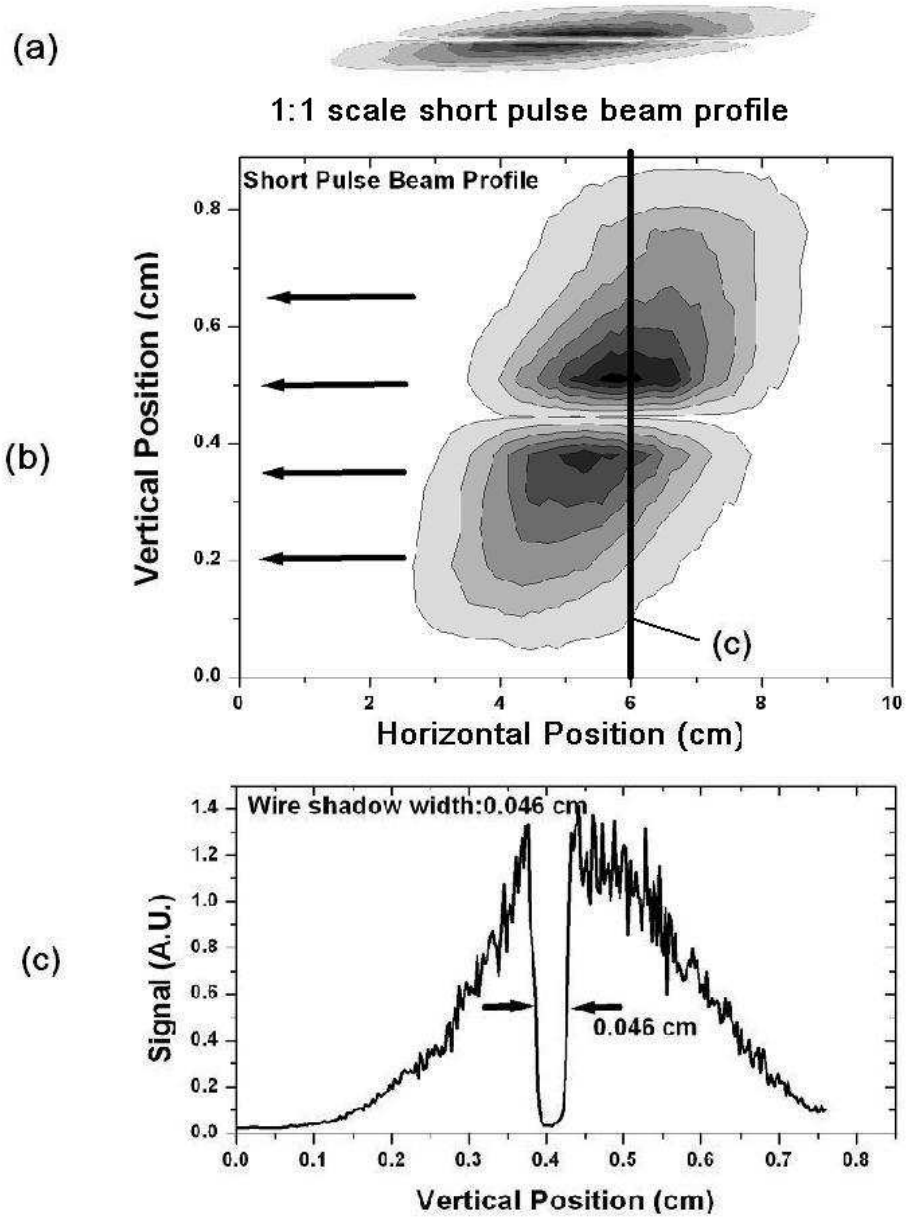

Figure A.4: Visualization of the short pulse beam:(a)1:1 scale contour map; (b)amplified contour map not in scale; (c)Vertical scan profile.

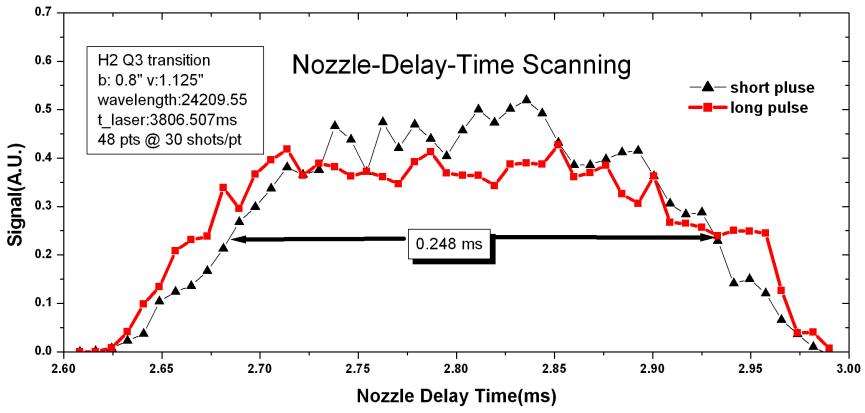

Figure A.5: Nozzle firing delay time scan. Data in long pulse mode (solid red square) and in short pulse mode (solid black triangle).

is 135 times smaller than that of the unpumped molecules (short pulse) shown in figureA.2. The first peak in Fig. A.6 corresponds to the incident (v=1, j=1) molecules. The second peak corresponds to the elastically scattered molecules from the Si(100) surface.

Another aspect related to the pumped molecular signal is the wavelength dependence. This was done with a wavelength scan. The data in Fig. A.7 show a FWHM of 0.0065 nm (equal to 0.258 in our DYE laser counting).

Several time scales related to the H_2 pulsed molecular beam: beam from the nozzle (248 μs), chopped beam (long mode:111.5 μs, short mode:7.3 μs), pumped beam (0.054 μs), are explained here. All the data above can be used as a quick reference for future work.

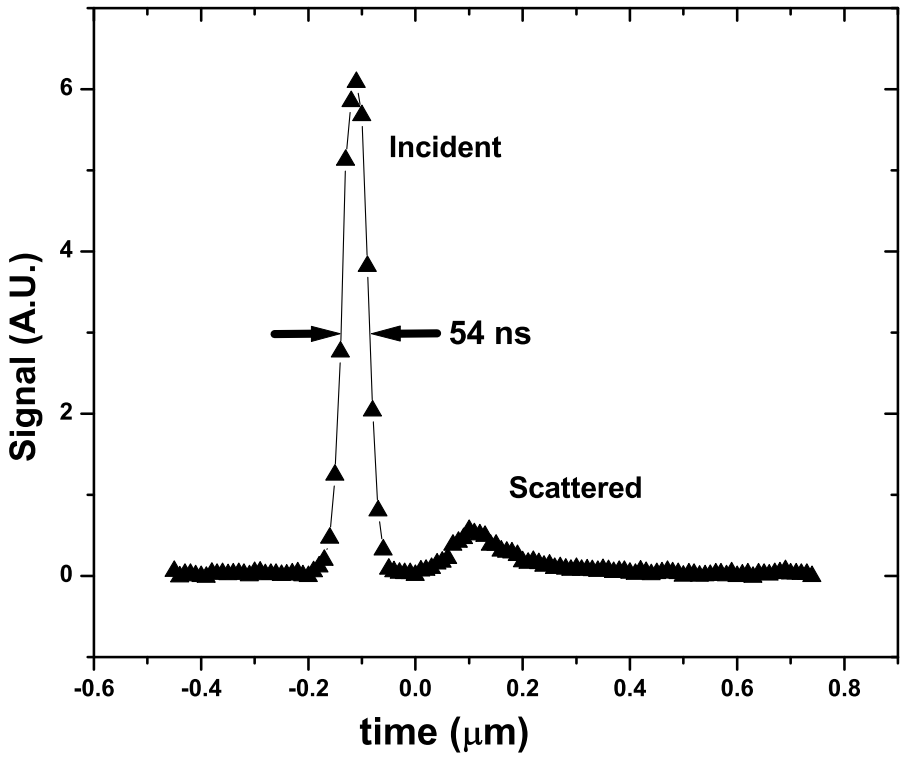

Figure A.6: TOF of (v=1,j=1) H_2 molecules incident on and scattered from Si(100).

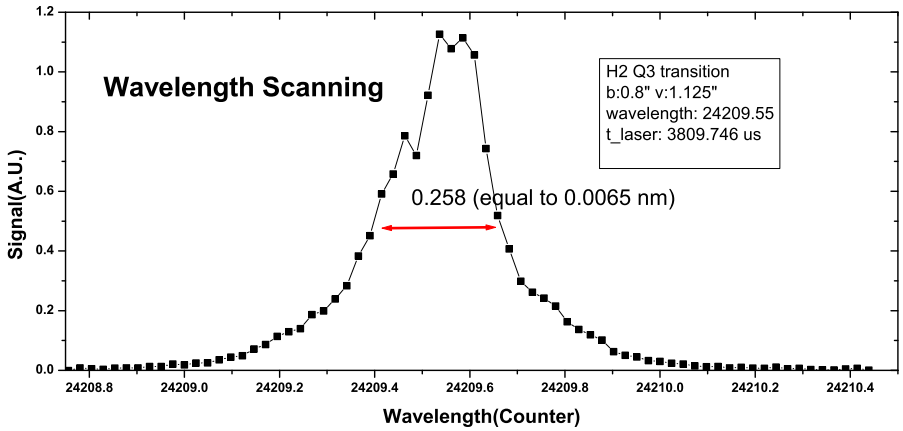

Figure A.7: Wavelength scan for (v=0, j=3) H_2 transition.

Appendix B

Convolution Based profile fitting and Density to Flux Transformation of TOF spectra

Considering the incident molecular beam as input to the scattering system and scattered molecular beam as output of the system, it is very natural to think that the scattering process is a linear time-invariant (LTI) system[1]. In LTI system theory the system can be characterized entirely by a single function - the system's impulse response function. The output of the system is simply the convolution of the input to the system with the system's impulse response function.

In our studies, first we constructed a density-weighted impulse response function $h_d(t)$ for the scattered signal which is the output of the incident molecules with zero spread in arrival time at the target, say, a delta function $\delta(t - t_0^{inc})$. The observed density-weighted spectra are the convolutions of the impulse response function $h_d(t)$ with the real incident signal $S(t)$, that is set to a Gaussian function whose height and width match those of the measured

[1] A LTI system has two properties: linearity and time invariance. Linearity means that if input $x_1(t)$ produces response $y_1(t)$ and $x_2(t)$ input produces response $y_2(t)$ then the scaled and summed input $ax_1(t) + bx_2(t)$ produces response $ay_1(t) + by_2(t)$ where a and b are real scalars. Time invariance means that if the output from input $x(t)$ is $y(t)$, then the output from input $x(t - T)$ is $y(t - T)$.

incident pulse. So far we don't know the details of the angular/velocity distributions of scattered molecules, that is the questions we want to answer. Also, due to the complexity of the signal involving many integrals and convolutions in both spatial and temporal dimensions, no explicit function is available for the exact impulse response function. The function for $h_d(t)$ is chosen to model the observations with a set of parameters, and the parameters are optimized by non-linear least square method to fit the measured spectrum. After the convolution based profile fitting is done, the experimental data are reproduced by a smoothed function which is used to extract the peak time. The peak times are used for calculating the mean translational energies or speed, the surface position and peak collision time as introduced in text.

After we have all this information, the density-weighted impulse response function multiplied by $\frac{v_{\perp}^{scat}(t)}{v_{inc}}$ is transformed into a flux-weighted impulse response function. Fluxes are defined differently in various research fields. As far as the question we studied is concerned, Flux = density $\times$ velocity. Absolute Survival Probability is the ratio of number of scattered molecules to that of incident molecules in the same quantum state. The impulse function is scaled by v_{inc} and weighted by $v_{\perp}^{scat}(t)$. v_{inc} is equal to the mean incident molecules' speed due to narrow velocity spread. $v_{\perp}^{scat}(t)$ is calculated by dividing the distance between probe laser and sample surface by the travel time. Only $v_{\perp}^{scat}(t) = v \cdot \cos(\theta)$, the projection of a scattered molecule's velocity onto the beam axis, is counted to calculate the flux flowing through the surface perpendicular to the beam axis.

Finally it is straightforward to calculated the flux-weighted spectra by reconvolving the flux-weighted impulse response function with $S(t)$.

Figure B.1 shows the optimized density-weighted impulse response function and the corresponding flux-weighted impulse response function. Note that the flux impulse function value is increased/decreased for the fast/slow molecules. That is also reflected in the TOF spectra as shown in Fig. B.2. We use the convolution fitting result, density-weighted spectrum, to find the peak time and the transformed result, flux-weighted spectrum, to calculate absolute survival probability. Also a Gaussian fit is presented in the graph to show the deviation from the experimental data[2].

In summary[3][4],

1. Construct density-weighted impulse response function (matlab file name: impluse_fun.m):

   6 parameters (p_1, p_2, p_3, p_4, p_5, p_6) are used to define the density-weighted impulse response function.

[2]A Gaussian function can well fit the incident peak but not the scattered peak especially for H_2/Si system due to the broad angular distribution

[3]Modified from matlab source codes for clarity. $S(t)$: incident beam TOF spectrum; $h_d(t)$: density-weighted impulse response function; $h_f(t)$: flux-weighted impulse response function; $y_d(t)$: scattered beam density-weighted TOF spectrum; $y_f(t)$: scattered beam flux-weighted TOF spectrum.

[4]Three Matlab scripts are written to solve the three main problems: 1, translational energy change for excited H_2(v=1, j=1); 2, absolute survival probability for excited H_2(v=1, j=1); 3, Monte Carlo method for ground H_2(v=0, j=1). The files' names are "scatter_energyloss.m", "scatter_surv.m" and "scatter_ground.m" respectively.

$$h_d(t) = \begin{cases} p_2 \frac{-(t-p_1)}{\{p_3[1+(t-p_4)^2]\}^2} & \text{t}< p_1 \\ \\ p_2 \frac{-(t-p_1)}{\{p_5[1+(t-p_6)^2]\}^2} & \text{t}\geq p_1 \end{cases} \tag{B.1}$$

2. Convolution of density-weighted impulse function with incident Gaussian function (matlab function name: my_cov.m):

$$y_d(t) \equiv S(t) * h_d(t) = \int_{-\infty}^{+\infty} S(t-\tau) \cdot h_d(\tau)\, \mathrm{d}\tau \tag{B.2}$$

3. Optimize 6 parameters using non-linear least square method (matlab function name: createFit_scatter_conv.m):

4. Density-weighted impulse response is obtained and transformed into flux-weighted impulse response (matlab function name: impulse_fun_DTF.m):

$$h_f(t) = h_d(t)\, \frac{v_{\perp}^{scat}(t)}{v_{inc}} \tag{B.3}$$

5. Density-weighted spectra and flux-weighted spectra are obtained by convolving corresponding impulse functions with incident beam profile (matlab function name: fitting_result_DTF.m):

$$y_f(t) \equiv S(t) * h_f(t) = \int_{-\infty}^{+\infty} S(t-\tau) \cdot h_f(\tau)\, \mathrm{d}\tau \tag{B.4}$$

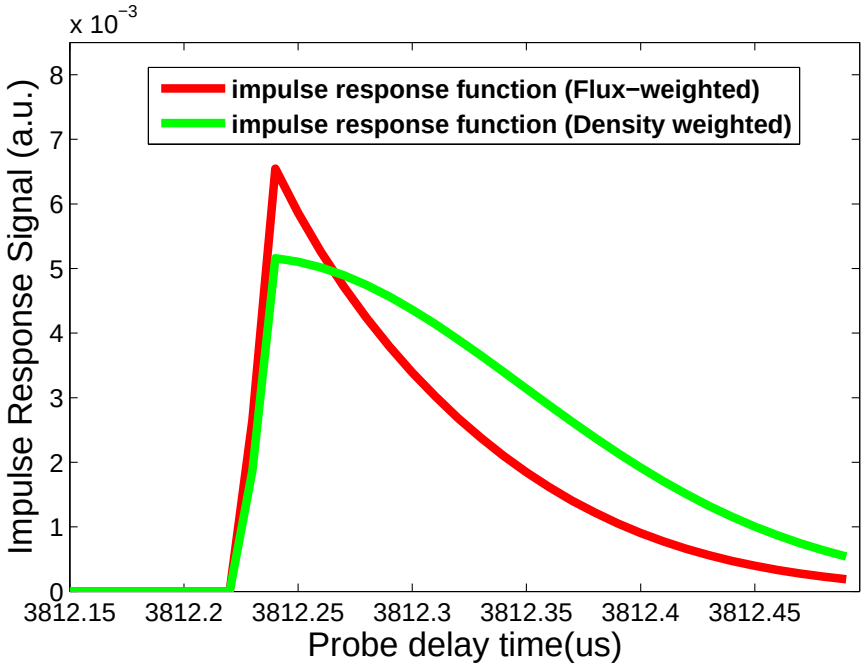

Figure B.1: Examples of density-weighted impulse response function (green) and the corresponding flux-weighted impulse response function(red) for input function $\delta(t - 3812.0247\ \mu s)$. Peak time of incident molecules: 3812.0247 μs; Probe laser postion: 0.6380 in; Sample position: 0.6255 in; Surface Temperature: 384 K.

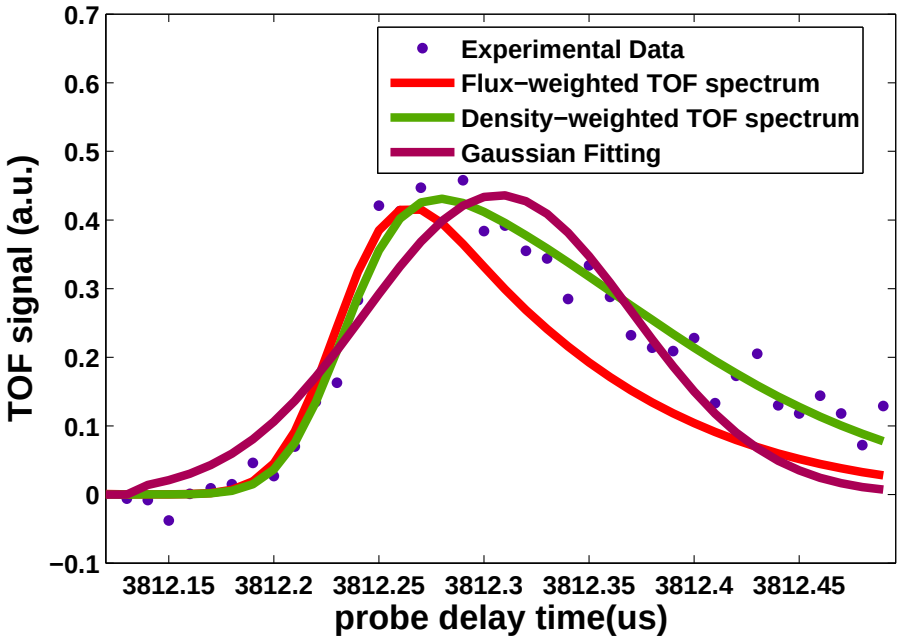

Figure B.2: Example of density to flux transformation of TOF spectrum. Convolution Fitting result (green),density-weighted spectrum, is used for finding the peak time; Transforming result, flux-weighted spectrum (red), is used for absolute survival probability calculation; also a Gaussian fit (purple) is presented in the graph to show the deviation from the experimental data. The same data set from Fig. B.1.

Appendix C

Monte Carlo simulation Based profile fitting Methods

Using the procedure described in section 2.3.2, the sample surface position shift doesn't affect the TOF spectra of H_2(v=0,j=1), that is to say, it is completely defined by pump and probe laser position. It is possible to extract the kinematic parameters of the scattered molecules by just analyzing the TOF spectra profile. Basically, the TOF spectra are results of multi-dimensional integral over spatial and temporal space. But it is difficult to solve the problem by numerical integrals. Monte Carlo simulation can be considered one method to solve this kind of integral. It is straightforward but needs careful consideration of the model, which must be close to the physical reality. The model we proposed and introduced in the text involves many parameters. The function ("fs_pp_function_ground_sc.m")to implement the Monte Carlo simulation for the scattered molecules beam has a total of 16 parameters as shown in Table C.1:

The first four of these parameters (sensitivity[1], n, $\overline{v_s}$ and σ_{v_s}) are op-

[1]The TOF spectrum's overall amplitude doesn't contain any information of scattered molecules' angular and speed distributions. At this point, only the other three parameters are of interest to us.

Table C.1: Parameters used in Monte Carlo simulation for scattered molecular beam.

parameters	definitions	methods to obtain or sources	typical value
n	angular distribution "n"	fit to scattered TOF	fit
scattered_v	mean speed "$\overline{v_s}$"	fit to scattered TOF	fit
scattered_v_var	speed variance "σ_{v_s}"	fit to scattered TOF	fit
sensitivity	signal amplitude factor	fit to scattered TOF	fit
NUMBIN	number of data points	program preset value	60
NUMPTS	number of test molecules	program preset value	1000,000
pump_width	width of focused pump laser	MC fit to incident TOF	0.00267 in
pump_length	length of pump laser	equal to sample size	0.0045 m
pump_posi_b	pump laser horizontal position	experimental result	0.6181 in
pump_posi_h	pump laser vertical position	experimentalal result	1.1245 in
pump_time	pump laser firing time	experimental result	3812.154 μs
probe_width	width of focused probe laser	trivial preset value	0.0005 in
probe_posi_b	probe laser horizontal position	experiment preset value	0.6240 in
probe_posi_h	probe laser vertical position	experiment preset value	1.1245 in
probe_start_t	time scan starting time	program preset value	3812.1 μs
probe_step_t	time scan step	program preset value	0.01 μs

timized using non-linear least squares method to fit the scattered beam TOF spectrum.

From Fig. C.1 to C.3, we can see how the three kinematic parameters shape the TOF profiles independently[2]. n changes the rear part of the TOF profile only; $\overline{v_s}$ shifts the overall profile; while σ_{v_s} changes both the front and rear part. Based on these facts, we extracted the kinematic parameters from scattered molecules' TOF spectra.

[2]When one parameter is varied in each figure, all other parameters are kept constant with default values.

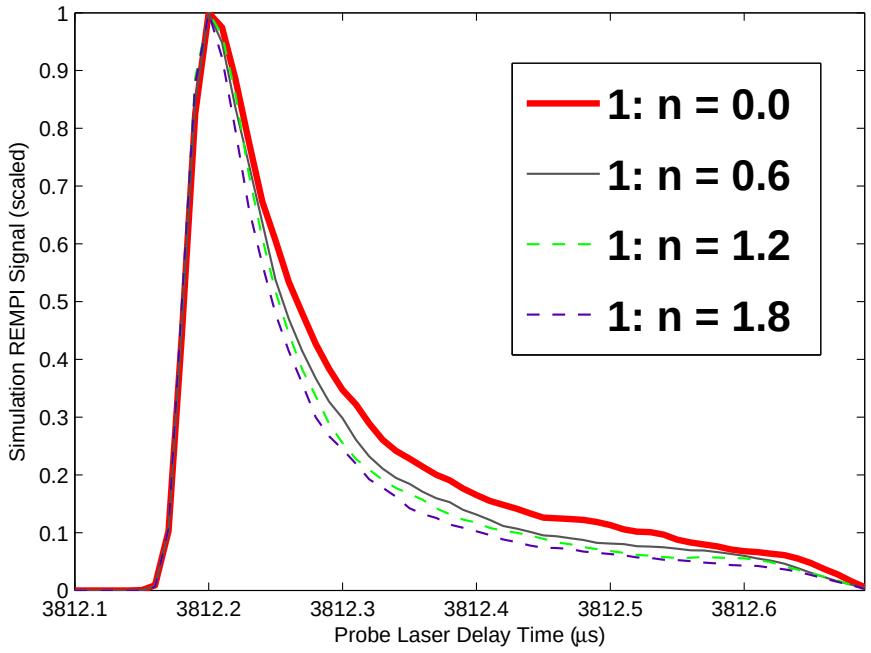

Figure C.1: Simulation TOF profiles versus angular distribution parameter n (Default values: $\overline{v_s}$=2540 m/s; σ_{v_s}=1000 m/s).

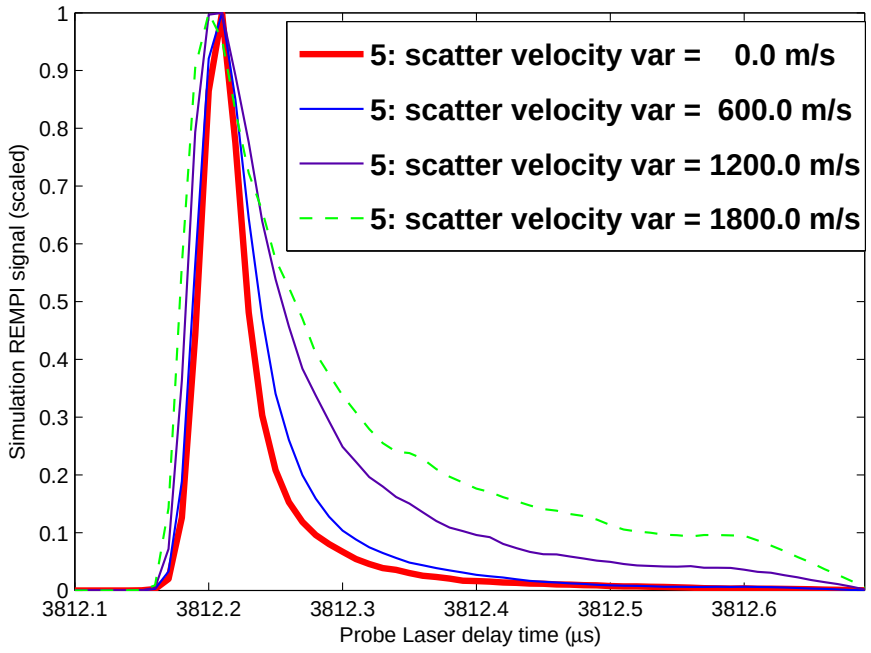

Figure C.2: Simulation TOF profiles versus scattered molecular speed variance σ_{v_s} (Default values: $n = 1$; $\overline{v_s}$=2540 m/s).

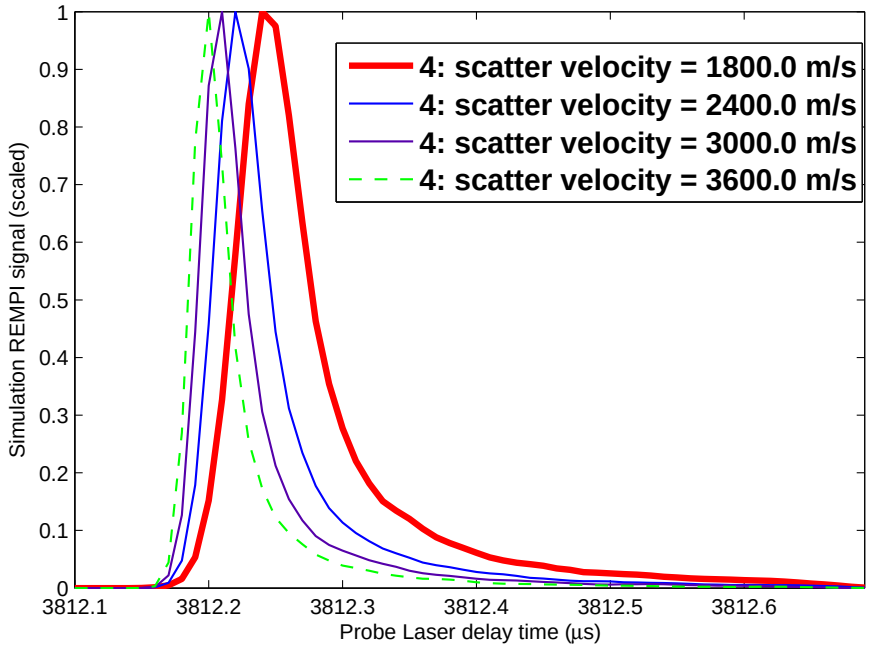

Figure C.3: Simulation TOF profiles versus mean scattered molecular speed $\overline{v_s}$ (Default values: $n = 1$; σ_{v_s}=1000 m/s).

Bibliography

[1] R. Bisson, L. Philippe, and M. Chātelet. Angle-resolved study of hydrogen abstraction on Si (1 0 0) and Si (1 1 1): Evidence for non-activated pathways. *Surface Science*, 600(19):4454–4463, 2006.

[2] J.J. Boland. Scanning tunnelling microscopy of the interaction of hydrogen with silicon surfaces. *Advances in Physics*, 42(2):129–171, 1993.

[3] P. Bratu, KL Kompa, and U. Höfer. Optical second-harmonic investigations of H_2 and D_2 adsorption on Si (100) 2x1: the surface temperature dependence of the sticking coefficient. *Chemical Physics Letters*, 251(1-2):1–7, 1996.

[4] RG Bray and RM Hochstrasser. Two-photon absorption by rotating diatomic molecules. *Molecular Physics*, 31(4):1199–1211, 1976.

[5] W. Brenig, A. Groß, and R. Russ. Detailed balance and phonon assisted sticking in adsorption and desorption of H_2/Si. *Zeitschrift für Physik B Condensed Matter*, 96(2):231–234, 1994.

[6] W. Brenig and MF Hilf. Reaction dynamics of H_2 and D_2 on Si (100) and Si (111). *Journal of Physics: Condensed Matter*, 13:R61, 2001.

[7] W. Brenig and E. Pehlke. Reaction dynamics of H_2 on Si. Ab initio supported model calculations. *Progress in Surface Science*, 83(5-6):263–336, 2008.

[8] YJ Chabal and K. Raghavachari. New ordered structure for the H-saturated Si (100) surface: the (3× 1) phase. *Physical Review Letters*, 54(10):1055–1058, 1985.

[9] DJ Chadi. Atomic and electronic structures of reconstructed Si (100) surfaces. *Physical Review Letters*, 43(1):43–47, 1979.

[10] CC Cheng and JT Yates Jr. H-induced surface restructuring on Si (100): Formation of higher hydrides. *Physical Review B*, 43(5):4041–4045, 1991.

[11] Y.W. Chung. *Practical guide to surface science and spectroscopy*. Academic Pr, 2001.

[12] M. Dürr and U. Höfer. Dissociative adsorption of molecular hydrogen on silicon surfaces. *Surface Science Reports*, 61(12):465–526, 2006.

[13] M. Gostein. *Dynamical Effects in Dissociative Adsorption: Quantum State-Resolved Studies of H_2 Scattering from Pd and Cu*. University of Texas at Austin, 1997.

[14] M. Gostein, H. Parhikhteh, and G.O. Sitz. Survival Probability of H_2(v= 1, J= 1) Scattered from Cu (110). *Physical Review Letters*, 75(2):342–345, 1995.

[15] M. Gostein and G.O. Sitz. Scattering of H_2(v= 1, J= 1) from Cu (110): Survival probability versus incident energy. *Journal of Vacuum Science Technology A: Vacuum, Surfaces, and Films*, 14(3):1562–1565, 1995.

[16] J. Greenwood. The correct and incorrect generation of a cosine distribution of scattered particles for Monte-Carlo modelling of vacuum systems. *Vacuum*, 67(2):217–222, 2002.

[17] D. Haneman. Surfaces of silicon. *Reports on Progress in Physics*, 50:1045, 1987.

[18] U. Höfer, L. Li, and TF Heinz. Desorption of hydrogen from Si (100) $2\times$ 1 at low coverages: The influence of π-bonded dimers on the kinetics. *Physical Review B*, 45(16):9485–9488, 1992.

[19] XF Hu, Z. Xu, D. Lim, MC Downer, PS Parkinson, B. Gong, G. Hess, and JG Ekerdt. In situ optical second-harmonic-generation monitoring of disilane adsorption and hydrogen desorption during epitaxial growth on Si (001). *Applied Physics Letters*, 71:1376, 1997.

[20] K. Inoue, Y. Morikawa, K. Terakura, and M. Nakayama. Order-disorder phase transition on the Si (001) surface: Critical role of dimer defects. *Physical Review B*, 49(20):14774–14777, 1994.

[21] J.M. Jasinski and S.M. Gates. Silicon chemical vapor deposition one step at a time: fundamental studies of silicon hydride chemistry. *Accounts of Chemical Research*, 24(1):9–15, 1991.

[22] N. Jedrecy, M. Sauvage-Simkin, R. Pinchaux, J. Massies, N. Greiser, and VH Etgens. Asymmetric versus symmetric dimerization on the Si (001) and As/Si (001) 2x1 reconstructed surfaces as observed by grazing incidence X-ray diffraction. *Surface Science*, 230(1-3):197–204, 1990.

[23] Jonghyuk Jim. *Quantum State-Resolved Studies of Sticking and Elastic Scattering of H_2 From Cu(100)*. University of Texas at Austin, 2006.

[24] K.W. Kolasinski. *Surface science: foundations of catalysis and nanoscience*. John Wiley & Sons Inc, 2008.

[25] K.W. Kolasinski, W. Nessler, A. de Meijere, and E. Hasselbrink. Hydrogen adsorption on and desorption from Si: Considerations on the applicability of detailed balance. *Physical Review Letters*, 72(9):1356–1359, 1994.

[26] Y. Kondo, T. Amakusa, M. Iwatsuki, and H. Tokumoto. Phase transition of the Si (001) surface below 100 K. *Surface Science*, 453(1-3):L318–L322, 2000.

[27] P. Krüger and J. Pollmann. Ab initio calculations of Si, As, S, Se, and Cl adsorption on Si (001) surfaces. *Physical Review B*, 47(4):1898–1910, 1993.

[28] M. Kubota and Y. Murata. Streak patterns in low-energy electron diffraction on Si (001). *Physical Review B*, 49(7):4810–4814, 1994.

[29] E. Landemark, CJ Karlsson, Y.C. Chao, and RIG Uhrberg. Dimer structure of the Si (001) (2x1) and c (4x2) reconstructions derived from core-level and valence-band photoemission results. *Surface Science*, 287:529–533, 1993.

[30] J.T. Law. Adsorption of hydrogen on silicon. *The Journal of Chemical Physics*, 30:1568, 1959.

[31] JE Lennard-Jones. Processes of adsorption and diffusion on solid surfaces. *Transactions of the Faraday Society*, 28:333–359, 1932.

[32] J.D. Levine. Structural and electronic model of negative electron affinity on the Si/Cs/O surface. *Surface Science*, 34(1):90–107, 1973.

[33] M. Liehr, CM Greenlief, M. Offenberg, and SR Kasi. Equilibrium surface hydrogen coverage during silicon epitaxy using SiH. *Journal of Vacuum Science & Technology A: Vacuum, Surfaces, and Films*, 8:2960, 1990.

[34] EE Marinero, CT Rettner, and RN Zare. Quantum-state-specific detection of molecular hydrogen by three-photon ionization. *Physical Review Letters*, 48(19):1323–1326, 1982.

[35] AJ Mayne, D. Riedel, G. Comtet, and G. Dujardin. Atomic-scale studies of hydrogenated semiconductor surfaces. *Progress in Surface Science*, 81(1):1–51, 2006.

[36] MS Mizielinski, DM Bird, M. Persson, and S. Holloway. Electronic nonadiabatic effects in the adsorption of hydrogen atoms on metals. *The Journal of chemical physics*, 122:084710, 2005.

[37] R. Nix. An Introduction to Surface Chemistry. *Online tuturial http://www.chem.qmul.ac.uk/surfaces/scc/*, 2003.

[38] J.E. Northrup. Electronic structure of Si (100) c (4× 2) calculated within the GW approximation. *Physical Review B*, 47(15):10032–10035, 1993.

[39] W. O'Mara, R.B. Herring, and L.P. Hunt. *Handbook of semiconductor silicon technology*. Crest Publishing House, South Africa, 2007.

[40] L. Perdigao, D. Deresmes, B. Grandidier, M. Dubois, C. Delerue, G. Allan, and D. Stievenard. Semiconducting Surface Reconstructions of p-Type Si (100) Substrates at 5 K. *Physical Review Letters*, 92(21):216101, 2004.

[41] A. Ramstad, G. Brocks, and PJ Kelly. Theoretical study of the Si (100) surface reconstruction. *Physical Review B*, 51(20):14504–14523, 1995.

[42] G. Ranga Rao, Z.H. Wang, H. Watanabe, M. Aoyagi, and T. Urisu. A comparative infrared study of H_2O reactivity on Si (1 0 0)-(2× 1),(2× 1)-H,(1× 1)-H and (3× 1)-H surfaces. *Surface Science*, 570(3):178–188, 2004.

[43] W. Ranke and D. Schmeisser. Adsorption of water on a cylindrical silicon crystal. *Surface Science*, 149(2-3):485–499, 1985.

[44] MB Raschke and U. Höfer. Chemisorption energy of hydrogen on silicon surfaces. *Physical Review B*, 63(20):201303, 2001.

[45] R.Y. Rubinstein and D.P. Kroese. *Simulation and the Monte Carlo method*. Wiley-interscience, 2008.

[46] K. Sagisaka, D. Fujita, and G. Kido. Phase Manipulation between c (4× 2) and p (2× 2) on the Si (100) Surface at 4.2 K. *Physical Review Letters*, 91(14):146103, 2003.

[47] T. Sakurai and H.D. Hagstrum. Interplay of the monohydride phase and a newly discovered dihydride phase in chemisorption of H on Si (100) 2× 1. *Physical Review B*, 14(4):1593–1596, 1976.

[48] RE Schlier and HE Farnsworth. Structure and adsorption characteristics of clean surfaces of germanium and silicon. *The Journal of Chemical Physics*, 30:917, 1959.

[49] L.C. Shackman. *Isotope Effects in Gas-Surface Interactions: Quantum-State Resolved Studies of D_2 Scattering from Cu (100) and Pd (111)*. University of Texas at Austin, 2004.

[50] L.C. Shackman and G.O. Sitz. State-to-state scattering of D_2 from Cu (100) and Pd (111). *The Journal of chemical physics*, 123:064712, 2005.

[51] G.O. Sitz. Gas surface interactions studied with state-prepared molecules. *Reports on Progress in Physics*, 65:1165, 2002.

[52] B.P. Stoicheff. On the dissociation energy of molecular hydrogen. *Canadian Journal of Physics*, 79(2-3):165–172, 2001.

[53] JR Trail, MC Graham, DM Bird, M. Persson, and S. Holloway. Energy loss of atoms at metal surfaces due to electron-hole pair excitations: First-principles theory of ąřchemicurrentsąś. *Physical Review Letters*, 88(16):166802, 2002.

[54] S. Ueno, Y. Narita, AR Khan, Y. Kihara, and A. Namiki. Scattering of 300 K effusive D_2 beams from the H/Si (1 0 0) surface. *Surface Science*, 602(8):1585–1588, 2008.

[55] Arban Uka. *Quantum State Resolved Studies of Copper-H_2 System and Electronic Spectroscopy of Cu(100)*. University of Texas at Austin, 2009.

[56] VA Ukraintsev, J.T. Yates, et al. The role of nickel in Si (001) roughening. *Surface Science*, 346(1-3):31–39, 1996.

[57] R. Walsh. Bond dissociation energy values in silicon-containing compounds and some of their implications. *Accounts of Chemical Research*, 14(8):246–252, 1981.

[58] H.N. Waltenburg and J.T. Yates Jr. Surface chemistry of silicon. *Chemical Reviews*, 95(5):1589, 1995.

[59] E. Watts. Quantum State-Resolved Studies of Elastic and Inelastic Scattering of H_2 from Cu and Pd. 1999.

[60] E. Watts and G.O. Sitz. State-to-state scattering in a reactive system: H_2(v= 1, J= 1) from Cu (100). *The Journal of Chemical Physics*, 114:4171, 2001.

[61] E. Watts, G.O. Sitz, DA McCormack, GJ Kroes, RA Olsen, JA Groeneveld, JNP Van Stralen, EJ Baerends, and RC Mowrey. Rovibrationally inelastic scattering of H_2(v= 1, j= 1) from Cu (100): Experiment and theory. *The Journal of Chemical Physics*, 114:495, 2001.

[62] A. Zangwill. *Physics at surfaces*. Cambridge Univ Pr, 1988.

[63] X.L. Zhou, CR Flores, and JM White. Adsorption and decomposition of water on Si (100): a TPD and SSIMS study. *Applied Surface Science*, 62(4):223–237, 1992.

Vita

Shengyuan Zhang was born in Taikang, Henan, P.R.China on Jan 31, 1977, the son of Yunchang Zhang and Cuifang Zhong. He received the B.S. M.A. in Physics from the Peking University, P.R.China in 2002. That same year he married Xu Hao. While at PKU his research area are in condense matter physics: research and applications of superconducting quantum interference device (SQUID). In the fall of 2002, he entered the Graduate School at The University of Texas, working in the laboratory of Prof. Greg Sitz studying the dynamics of molecule surface interaction using pulsed supersonic molecular bean and quantum state-specific detection techniques.

Permanent address: 20 Yellow River St. 34
Zhengzhou, Henan 450003
P.R.China

This dissertation was typeset with LaTeX[†] by the author.

[†]LaTeX is a document preparation system developed by Leslie Lamport as a special version of Donald Knuth's TeX Program.